Effects of magnetic field on thermo-hydraulic performance of Fe_3O_4-water nanofluids in a corrugated tube

Siyuan Mei [a], Cong Qi [a*], Tao Luo [a], Xinfeng Zhai [a], Yuying Yan [b*]

[a] School of Electrical and Power Engineering, China University of Mining and Technology, Xuzhou 221116, China

[b] Fluids & Thermal Engineering Research Group, Faculty of Engineering, University of Nottingham, Nottingham NG7 2RD, UK

Abstract:

An experimental system is established to investigate the thermo-hydraulic performance of Fe_3O_4-water nanofluids in a corrugated tube under various magnetic fields. The influences of magnetic induction intensities (B=0 G, 100 G, 200 G, 300 G), nanoparticle mass fractions (ω=0.0%, 0.1%, 0.3%, 0.5%), electromagnet arrangement modes (one-side electromagnet and two-side staggered electromagnet), kinds of tubes (smooth tube and corrugated tube), Reynolds numbers (Re=800-12000) on flow and heat transfer characteristics are discussed. It is obtained that the augmentation of heat transfer is more sensitive to high nanoparticle mass fraction, high magnetic induction intensity, two-side staggered electromagnet and corrugated tube. A Comprehensive evaluation index is applied to estimate the thermo-hydraulic performance. It can be discovered that the comprehensive evaluation index increases with the increasing Reynolds number at first and then decreases, and the rough surface of corrugated tube delays the appearance of critical Reynolds number.

Keywords: Nanofluids; Magnetic field; Corrugated tube; Heat transfer enhancement

*Correspondence author.
E-mail: meisiyuan@cumt.edu.cn (S. Mei), qicong@cumt.edu.cn (C. Qi), luotao@cumt.edu.cn (T. Luo), zhaixinfeng@cumt.edu.cn (X. Zhai), yuying.yan@nottingham.ac.uk (Y. Yan)

Nomenclature

A_c	cross-sectional area, m^2
B	magnetic induction intensity, G
c_p	specific heat of nanofluids, $J \cdot kg^{-1} \cdot K^{-1}$
c_{pbf}	specific heat of base fluid, $J \cdot kg^{-1} \cdot K^{-1}$
c_{pp}	specific heat of nanoparticle, $J \cdot kg^{-1} \cdot K^{-1}$
D_e	hydraulic diameter, m
D_c	nanoparticle size, m
f	frictional resistance coefficient of nanofluids
h	convective heat transfer coefficient, $W \cdot m^{-2} \cdot K^{-1}$
k	shape factor
L	length of tube, m
Nu	Nusselt number of nanofluids
$\Delta p/\Delta L$	pressure drop per unit length, $Pa \cdot m^{-1}$
P	wetted perimeter, m
p	pressure drop, Pa
q_m	mass flow rate, $kg \cdot s^{-1}$
Q_f	effective heating power, W
Re	Reynolds number
r_0	external diameter, m
r_i	inner diameter, m
T_{wo}	average temperature of outside wall, K
T_{wi}	average temperature of inside wall, K
T_{in}	inlet temperatures, K
T_{out}	outlet temperatures, K
T_f	average temperature of nanofluids, K
u	velocity of nanofluids, $m \cdot s^{-1}$

Greek symbols

ρ	density of nanofluids, $kg \cdot m^{-3}$
ρ_{bf}	density of base fluid, $kg \cdot m^{-3}$
ρ_p	density of nanoparticle, $kg \cdot m^{-3}$
φ	nanoparticle volume fraction, %
ω	nanoparticle mass fraction, %
δ	wall thickness of tube, m
λ	thermal conductivity of copper, $W \cdot m^{-1} \cdot K^{-1}$
λ_f	thermal conductivity of nanofluids, $W \cdot m^{-1} \cdot K^{-1}$
λ'	X-ray wavelength, Å
β	line broadening full width at half maximum (FWHM) of peak
θ	Bragg diffraction angle, rad
μ_f	dynamic viscosity of nanofluids, Pa·s
ζ	comprehensive evaluation index

Subscripts

bf	base fluid
f	nanofluids
p	nanoparticle
PP	same pumping power
w	wall

1 Introduction

The augmentation of heat transfer performance is an inevitable challenge in industry, active and passive heat transfer enhancement technologies can be adopted in heat exchangers [1, 2] and electronic components [3, 4, 5]. Active heat transfer enhancement technologies mainly include magnetic field [6, 7, 8], mechanical rotating and agitating [9]. Passive heat transfer enhancement technologies mainly

include improvement of thermophysical properties of working fluids [10, 11, 12], rough surface such as corrugated tube [13, 14, 15], internal and external thread tube [16, 17].

Due to the low thermal conductivity, some traditional working fluid, such as water and ethylene glycol, cannot meet the requirements of heat exchanger. On this background, nanofluids, as a kind of high thermal conductivity working fluid, have been used in many heat transfer fields, such as boiling heat transfer, convective heat transfer, photothermal conversion and photothermal conversion. For pool boiling heat transfer, Fan et al. conducted a study on the effects of length and diameter [18] on boiling heat transfer of carbon nanotube (CNT)-based aqueous nanofluids, also studied the influence of concentration on boiling heat transfer of graphene-based aqueous nanofluids [19] and aqueous nanofluids in the presence of graphene and graphene oxide nanosheets [20]. For convective heat transfer, Guo et al. [21] reported the heat transfer performance of nanofluids in a square cavity. Sheremet et al. investigated the influences of corner heater [22] and thermal dispersion [23] on the natural convection heat transfer of nanofluids. For photothermal conversion, Liu et al. [24, 25] reported the solar-thermal conversion of various nanospheres. Wang et al. [26] and Liu et al. [27] investigated the solar steam generation by carbon-nanotube and graphene oxide nanofluids respectively.

Based on the passive heat transfer enhancement technologies (nanofluids instead of water and ethylene glycol), some researchers have adopted active heat transfer enhancement technologies (adding magnetic field on nanofluids).

For free convection heat transfer, Sheikholeslami et al. [28] applied a two phase model to investigate the influence of magnetic field on the double diffusion convection of nanofluids. It was found that temperature gradient increases with the suction parameter but deteriorates with the Schmidt number, thermophoretic parameters and Brownian motion. Sheikholeslami et al. [29] numerically investigated the influence of magnetic field on an open porous cavity full of nanofluids by lattice Boltzmann method. It was discovered that natural convection heat transfer can be improved with the increasing Darcy number. Sheikholeslami et al. [30] conducted a research on free convection of an enclosure full of Fe_3O_4-water nanofluids under magnetic field. It was obtained that heat transfer performance decreases with Lorentz forces but increases with buoyancy forces. Sheikholeslami et al. [31] studied the effects of Lorenz forces on the free convection heat transfer of water based nanofluids. It was reported that the increasing Darcy number can reduce the thickness of the boundary layer but Hartmann number can increase it. In addition, Sheikholeslami et al. also investigated the natural convection heat transfer of nanofluids in porous enclosures by Darcy model [32], non-equilibrium model [33, 34], control volume based finite element method [35, 36] respectively.

For forced convection heat transfer, Sheikholeslami et al. [37] applied control volume based finite element method to analyze the forced convection heat transfer in a porous semi-annulus full of nanofluids considering the influences of the shape of nanoparticle and magnetic field. It was obtained that heat transfer performance decreases with Lorentz forces but increases with Darcy and Reynolds number.

Sheikholeslami et al. [38] numerically studied the forced convection in a cubic cavity full of nanofluids considering the magnetic field. It was obtained that the temperature gradient increases with velocity of moving surface but decreases with the Lorentz forces. Sheikholeslami et al. [39] numerically investigated the force convection heat transfer of nanofluids in a lid driven enclosure considering the influence of electric field. It was obtained that the flow style is related to the electric field, and Nusselt number increases with Coulomb forces. Sheikholeslami et al. [40] numerically studied the forced convection heat transfer of an enclosure filled with nanofluids considering variable properties and the influence of electric field. It was found that Coulomb force is beneficial to enhance the heat transfer. Sheikholeslami et al. [41] numerically simulated the forced convection heat transfer of an enclosure full of nanofluids considering moving and sinusoidal walls. It was obtained that heat transfer performance decreases with Hartmann number but increases with Reynolds number. Sheikholeslami et al. investigated the forced convection heat transfer of nanofluids in porous enclosures considering the Lorentz forces [42], Brownian motion [43, 44]. It was found that Hartmann number reduces the kinetic energy and convection heat transfer performance, and increases the temperature gradient.

Above researchers adopted the combination of nanofluids and magnetic field to improve the heat transfer, which promotes the heat transfer enhancement technology. However, the combination of nanofluids, magnetic field and rough surface (corrugated tube) is investigated less. Compared with smooth tube, corrugated tube not only has a larger heat exchange area when their hydraulic diameters are the same,

but also can destroy the laminar boundary layer by its cyclical peaks and troughs. Besides, corrugated tube is widely applied in industry and has a strong ability of self-descaling. Hence, the thermo-hydraulic performance of Fe_3O_4-water nanofluids in a corrugated tube under a magnetic field is experimentally investigated. The effects of magnetic induction intensities (B=0 G, 100 G, 200 G, 300 G), mass fractions of nanoparticle (ω=0.0%, 0.1%, 0.3%, 0.5%), electromagnet arrangement modes (one-side electromagnet and two-side staggered electromagnet), kind of tubes (smooth tube and corrugated tube), Reynolds numbers (Re=800-12000) on flow and heat transfer characteristics are researched. A Comprehensive evaluation index is applied to evaluate the thermo-hydraulic performance.

2 Experimental Method

2.1 Preparation of Fe_3O_4-water nanofluids and stability study

Two-step method is used to prepare Fe_3O_4-water nanofluids in this experiment. Fig. 1 presents the characteristics of nanoparticles and nanofluids. It can be found from scanning electron microscope (SEM), transmission electron microscope (TEM) photographs that nanoparticles easily gather together. It can be also found from X-Ray Diffraction (XRD) photographs that intensity of nanoparticles measured has a good agreement with the standard card of Fe_3O_4, which means the nanoparticles in this experiment is Fe_3O_4 nanoparticles. Based on equation (1), nanoparticle size is calculated and it is about 15nm, which is the same of the size provided by manufacturers. In order to prepare stable nanofluids, some dispersing agent (GA) is added into base fluid, the value of pH is adjusted into 8, and ultrasonic oscillation is

conducted about 40 minutes. It can be found that nanofluids still maintain good stability after 20 days.

Based on XRD, nanoparticle size equation can be calculated as follows:

$$D_c = \frac{k\lambda'}{\beta \cdot \cos\theta} \tag{1}$$

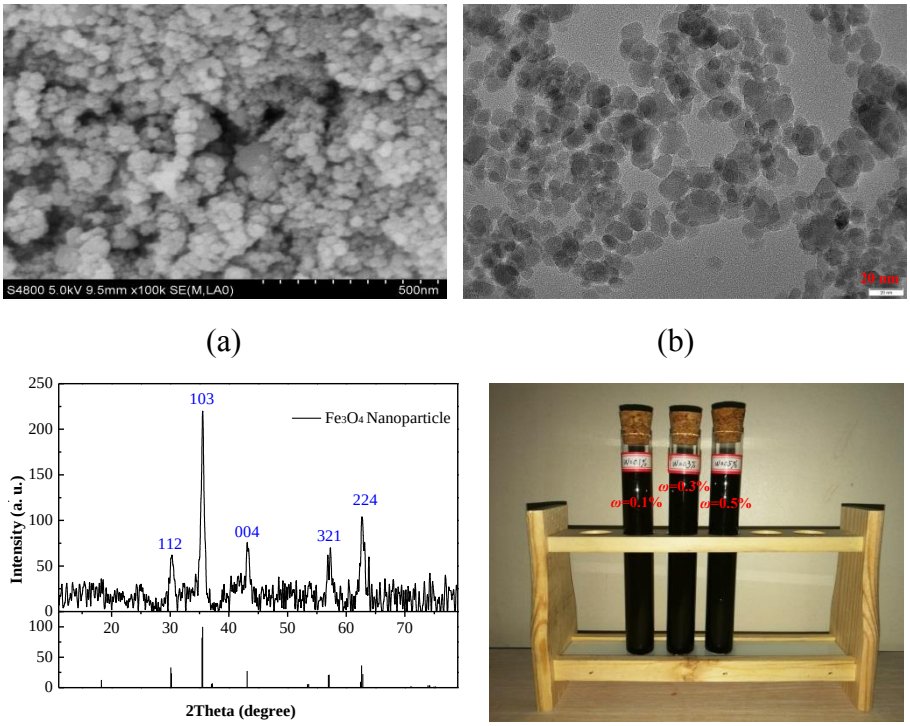

Fig. 1. Details of nanoparticles and Fe_3O_4-water nanofluids, (a) SEM, (b) TEM, (c) XRD, (d) nanofluids after standing 20 days

2.2 Experiment set

The schematic diagram of the experiment system is given in Fig. 2. For the heat transfer characteristics, in order to measure the surface temperatures, ten T-type thermocouples are uniformly distributed on the surface of tube. To avoid the entrance effects, each 100mm length is left at two ends of tube. The fluid inlet and outlet temperatures are measured by two thermocouples. In order to record the temperatures, a data acquisition instrument is necessary. Resistance wire wound around the tube is

connected to a power supply. To prevent heat loss, insulating layer is wrapped around the tube. For the flow characteristics, in order to measure the pressure drop, a differential pressure gauge is used in this experiment. A low-temperature thermostat bath is used to cool the working fluid. Fig. 3 shows the details of arrangement modes of electromagnets around the corrugated tube. One-side arrangement and two-side staggered arrangement are adopted in this experiment. The magnetic induction intensity is measured by a Gauss meter (TX-15). The length of corrugated tube is L=1.2m, and the diameter at the narrowest point of corrugated tube is D_{min}=0.009m, and the diameter at the widest point is D_{max}=0.013m. The wall thickness is δ=0.001m.

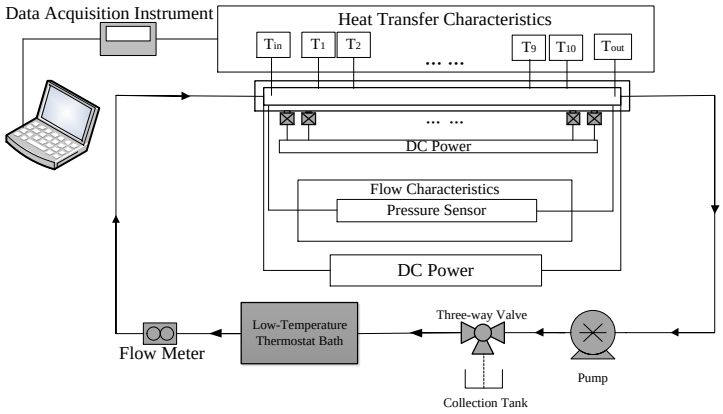

Fig. 2. Schematic diagram of experimental system

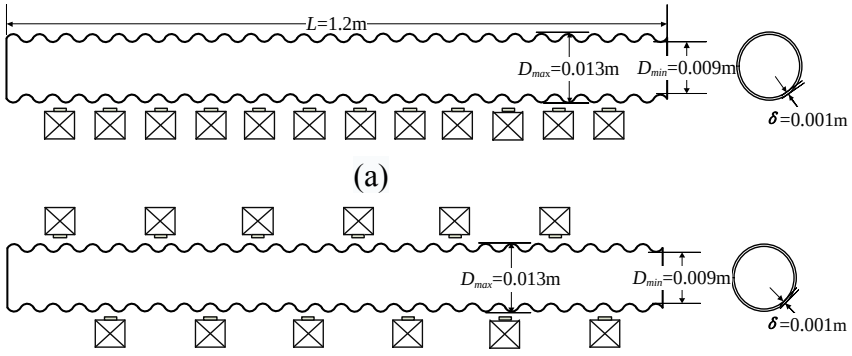

Fig. 3. Details of arrangement modes of electromagnets around the corrugated tube, (a) one-side arrangement, (b) two-side staggered arrangement

2.3 Uncertainty analysis

In order to guarantee the accuracy of experiment, it is indispensable to analyze the experimental uncertainty. The followings are the relevant equations for Nusselt number and resistance coefficient respectively [45]:

$$\frac{\delta Nu}{Nu}=\sqrt{(\frac{\delta Q_{\mathrm{f}}}{Q_{\mathrm{f}}})^2+(\frac{\delta T}{T})^2} \tag{2}$$

$$\frac{\delta f}{f}=\sqrt{(\frac{\delta p}{p})^2+(\frac{\delta L}{L})^2+(\frac{\delta q_{\mathrm{m}}}{q_{\mathrm{m}}})^2} \tag{3}$$

Table 1 shows the errors of each section in the experiment. The error of Nusselt number is ±5.0% and resistance coefficient is ±1.18%, which can make sure the experimental system accuracy.

Table 1 Errors of each section in the experiment

$\delta Q_{\mathrm{f}}/Q_{\mathrm{f}}$	$\delta T/T$	$\delta p/p$	$\delta l/l$	$\delta q_{\mathrm{m}}/q_{\mathrm{m}}$	$\delta Nu/Nu$	$\Delta f/f$
±5.0%	±0.1%	±0.5%	±0.1%	±1.06%	±5.0%	±1.18%

2.4 Experimental data analysis

The equivalent diameter of the corrugated tube can be calculated as follows:

$$D_{\mathrm{e}}=\frac{4A_{\mathrm{c}}}{P} \tag{4}$$

Reynolds number is calculated as follows:

$$Re=\frac{\rho u D_{\mathrm{e}}}{\mu_{\mathrm{f}}} \tag{5}$$

The heat transfer capacity between tube wall and fluid can be calculated as follows:

$$Q_{\mathrm{f}}=c_{\mathrm{p}}q_{\mathrm{m}}(T_{\mathrm{out}}-T_{\mathrm{in}}) \tag{6}$$

Specific heat and density of nanofluids can be calculated as follows [46]:

$$c_{\mathrm{p}}=(1-\varphi)c_{\mathrm{pbf}}+\varphi c_{\mathrm{pp}} \tag{7}$$

$$\rho = (1-\varphi)\rho_{\mathrm{bf}} + \varphi\rho_{\mathrm{p}} \tag{8}$$

Average temperature of nanofluids is calculated by the following equation:

$$T_{\mathrm{f}} = \frac{T_{\mathrm{in}} + T_{\mathrm{out}}}{2} \tag{9}$$

Average temperature of the outside wall can be calculated as follows:

$$T_{\mathrm{wo}} = [\sum_{i=1}^{10} T_{\mathrm{wo}}(i)] / 10 \tag{10}$$

Average temperature of the inside wall can be calculated by the following equation:

$$T_{wi} = T_{\mathrm{wo}} - \frac{Q_{\mathrm{f}} \ln(r_{\mathrm{o}} / r_i)}{2\pi\lambda L} \tag{11}$$

Convective heat transfer coefficient can be calculated as follows:

$$h = \frac{Q_{\mathrm{f}}}{\pi D_{\mathrm{e}} L (T_{wi} - T_{\mathrm{f}})} \tag{12}$$

The definition of Nusselt number is as follows:

$$Nu = \frac{hD_e}{\lambda_{\mathrm{f}}} \tag{13}$$

The definition of frictional resistance coefficient is as follows:

$$f = \frac{2D_{\mathrm{e}}}{\rho u^2} \cdot \frac{\Delta p}{\Delta L} \tag{14}$$

More nanoparticles not only cause higher thermal conductivity but also higher flow resistance. For the heat transfer enhancement, flow resistance augment and the thermal conductivity enhancement are two opposite factors. In order to analyze the thermo-hydraulic performance, a comprehensive evaluation index is used in this paper as follows [17]:

$$\xi = \left(\frac{Nu}{Nu_{\mathrm{bf+circular\ tube}}} \right) \Big/ \left(\frac{f}{f_{\mathrm{bf+circular\ tube}}} \right)^{\frac{1}{3}} \tag{15}$$

3 **Results and discussions**

3.1 Experimental system verification

A validation experiment is conducted to guarantee the dependability of the experimental system. By comparing experimental results with other results obtained by published references [46, 47, 48, 49], Fig. 4 shows that the errors of both Nusselt number and resistance coefficient are within 4.9%, which can ensure the reliability of the experimental system.

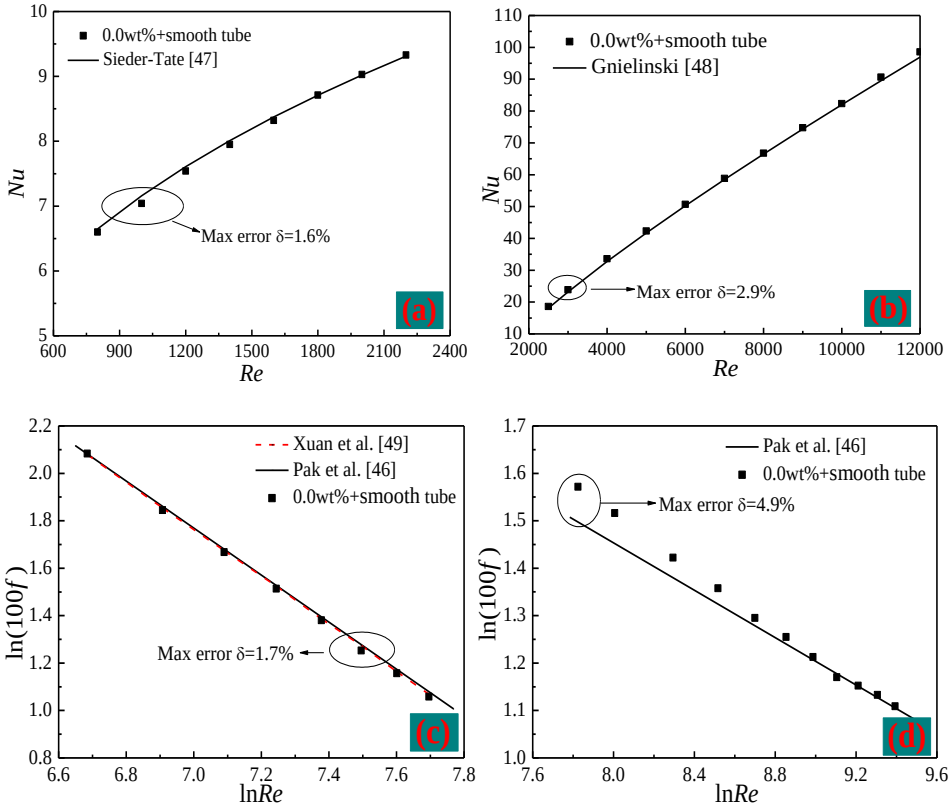

Fig. 4. Comparison between the experimental results and other results obtained by published references, *Nu*: (a) laminar flow, (b) turbulent flow; *f*: (c) laminar flow, (d) turbulent flow

3.2 Experimental results and discussions

3.2.1 Nusselt number

3.2.1.1 Effect of nanoparticle mass fraction

The influence of nanoparticle mass fraction on Nusselt number is investigated

for smooth tube and corrugated tube respectively with the same magnetic induction intensity and electromagnet arrangement mode.

Fig. 5 shows the influences of nanoparticle mass fractions on Nusselt numbers of smooth tube with one-side electromagnets. For laminar flow, it can be found that Nusselt number of nanofluids can be improved by 4.1%, 6.1%, 8.0%, 9.2% at best compared with water under B=0 G, 100 G, 200 G and 300 G respectively. For turbulent flow, it can be found that Nusselt number of nanofluids can be improved by 8.5%, 11.0%, 13.5%, 15.7% at best compared with water under B=0 G, 100 G, 200 G and 300 G respectively. The heat transfer is improved remarkably when using nanofluids. It can be concluded that the increase of nanoparticle mass fraction leads to the augment of Nusselt number. All these are due to the higher thermal conductivity and more intense Brownian motion of nanoparticles compared with water. The reduction of thermal resistance caused by the increasing nanoparticle mass fraction (increasing thermal conductivity) is beneficial to heat transfer enhancement. Besides, Brownian motion of nanoparticles can destroy the laminar boundary layer, which can reduce the thermal resistance of heat transfer between tube and nanofluids. It can be also found that the enhancement ratio in turbulent flow is larger than that in laminar flow. It is because that viscosity is the major negative factor for heat transfer enhancement in laminar flow, while in turbulent flow, the Brownian motion and thermal conductivity are the main factors to enhance the heat transfer.

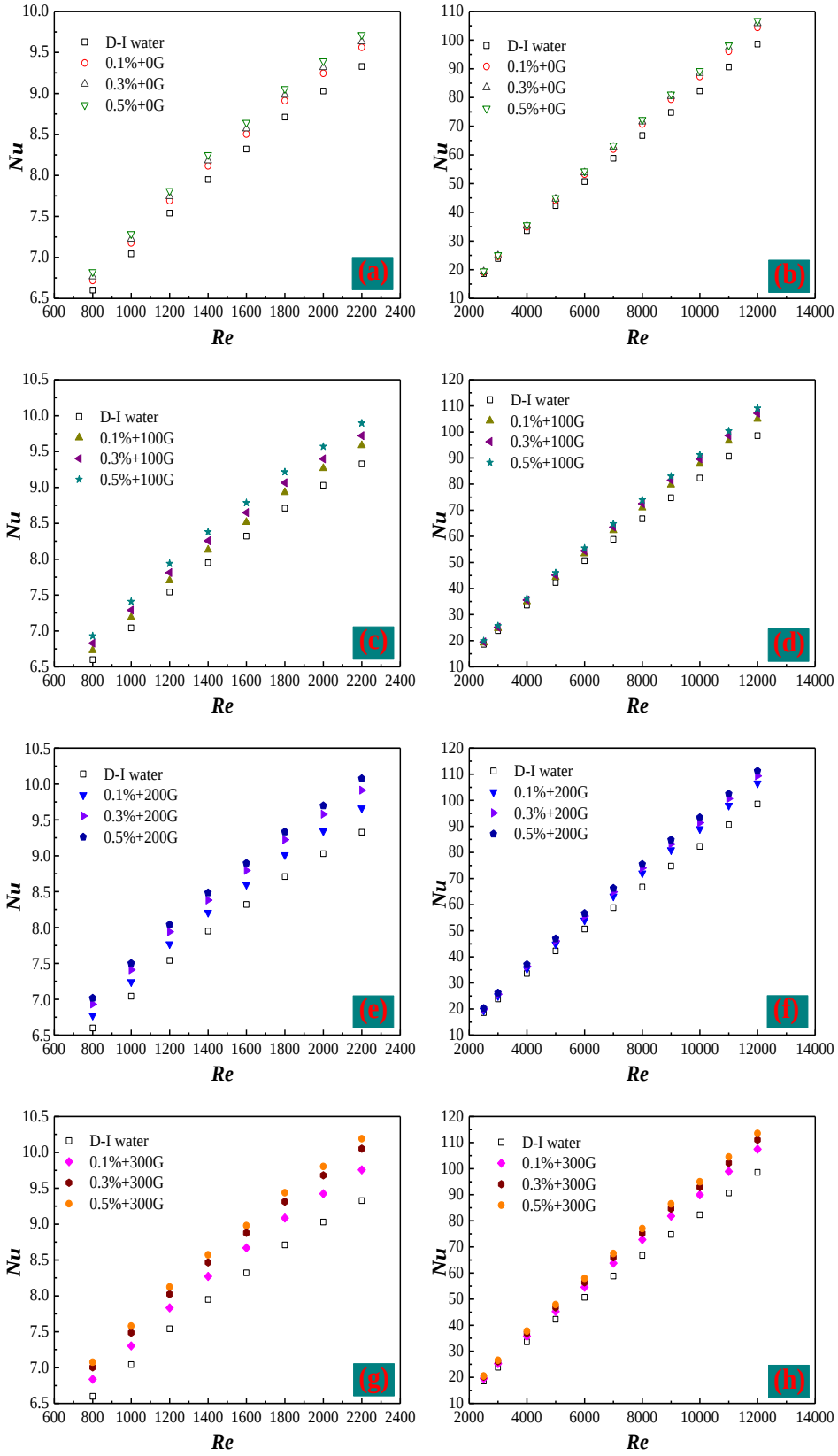

Fig. 5. Effects of nanoparticle mass fractions on Nusselt numbers of smooth tube with one-side electromagnets. (a) 0G+laminar flow, (b) 0G+turbulent flow, (c) 100G +laminar flow, (d) 100G+turbulent flow, (e) 200G+laminar flow, (f) 200G+turbulent flow,(g) 300G+laminar flow, (h) 300G+turbulent flow

Fig. 6 shows the influences of nanoparticle mass fractions on Nusselt numbers of smooth tube with two-side staggered electromagnets. For laminar flow, it can be found that Nusselt number of nanofluids can be improved by 4.1%, 7.7%, 8.9%, 10.1% at best compared with water under B=0 G, 100 G, 200 G and 300 G respectively. For turbulent flow, it can be found that Nusselt number of nanofluids can be improved by 8.5%, 12.9%, 15.4%, 17.6% at best compared with water under B=0 G, 100 G, 200 G and 300 G respectively.

Fig. 7 gives the effects of nanoparticle mass fractions on Nusselt numbers of corrugated tube with one-side electromagnets. For laminar flow, it can be found that Nusselt number of nanofluids can be improved by 2.4%, 4.1%, 5.4%, 6.5% at best compared with water under B=0 G, 100 G, 200 G and 300 G respectively. For turbulent flow, it can be found that Nusselt number of nanofluids can be improved by 4.4%, 6.2%, 7.5%, 8.9% at best compared with water under B=0 G, 100 G, 200 G and 300 G respectively.

Fig. 8 presents the effects of nanoparticle mass fractions on Nusselt numbers of corrugated tube with two-side staggered electromagnets. For laminar flow, it can be found that Nusselt number of nanofluids can be improved by 2.4%, 5.3%, 6.4%, 7.2% at best compared with water under B=0 G, 100 G, 200 G and 300 G respectively. For turbulent flow, it can be found that Nusselt number of nanofluids can be improved by 4.4%, 7.3%, 8.6%, 10.0% at best compared with water under B=0 G, 100 G, 200 G and 300 G respectively.

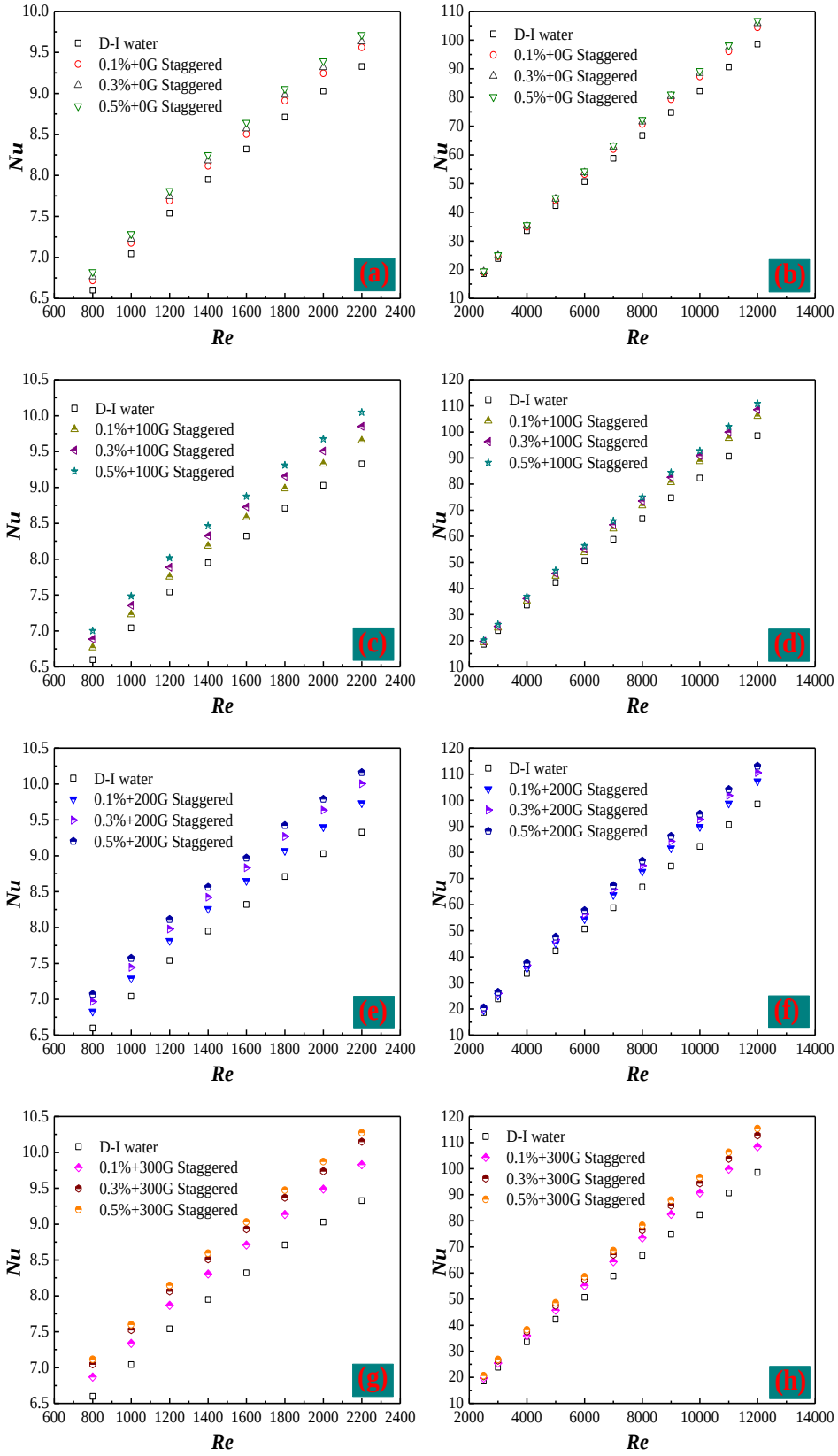

Fig. 6. Effects of nanoparticle mass fractions on Nusselt numbers of smooth tube with two-side staggered electromagnets. (a) 0G+laminar flow, (b) 0G+turbulent flow, (c) 100G+laminar flow, (d) 100G+turbulent flow, (e) 200G+laminar flow, (f) 200G+turbulent flow,(g) 300G+laminar flow, (h) 300G+turbulent flow

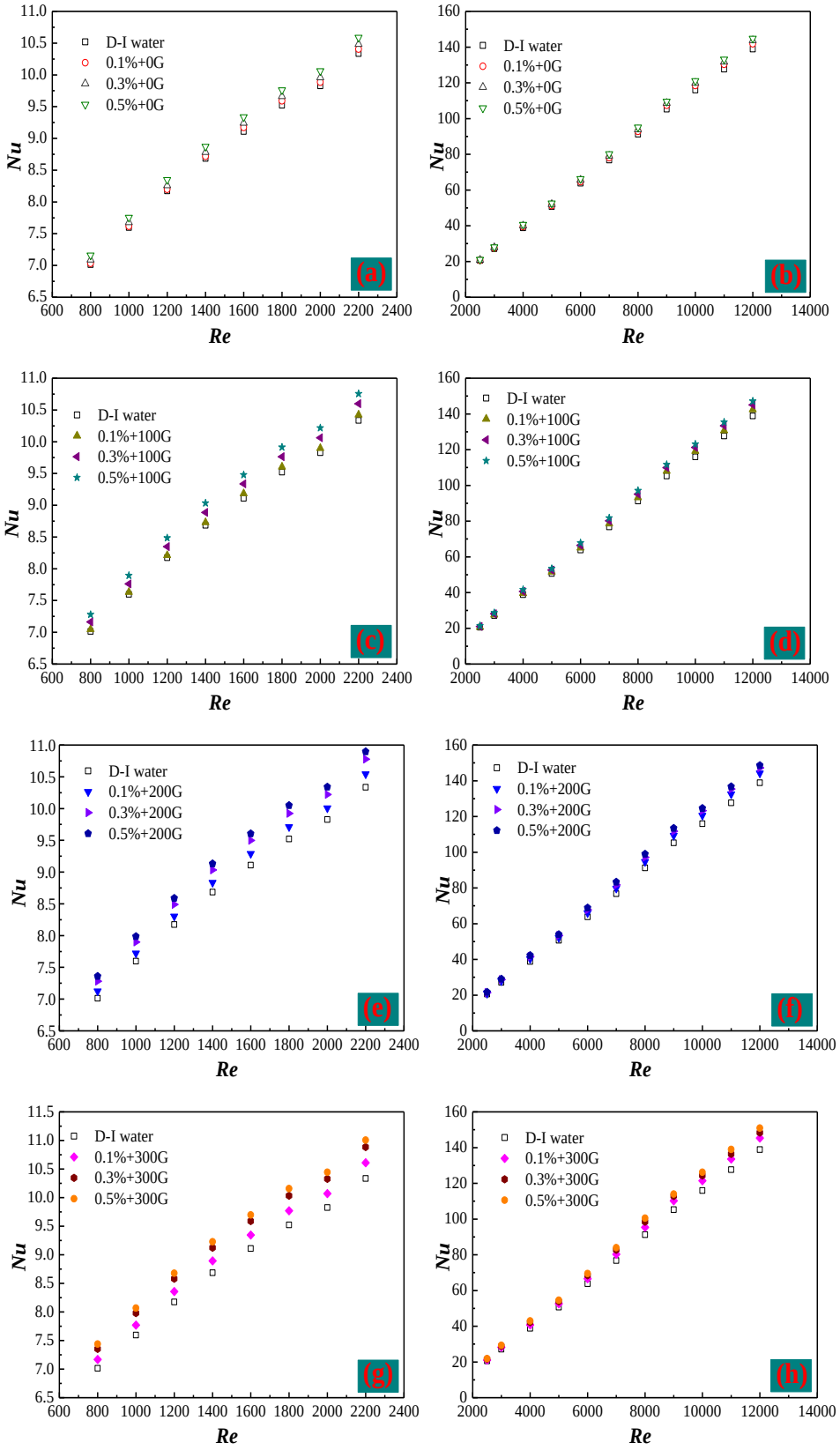

Fig. 7. Effects of nanoparticle mass fractions on Nusselt numbers of corrugated tube with one-side electromagnets. (a) 0G+laminar flow, (b) 0G+turbulent flow, (c) 100G+laminar flow, (d) 100G+turbulent flow, (e) 200G+laminar flow, (f) 200G+turbulent flow,(g) 300G+laminar flow, (h) 300G+turbulent flow

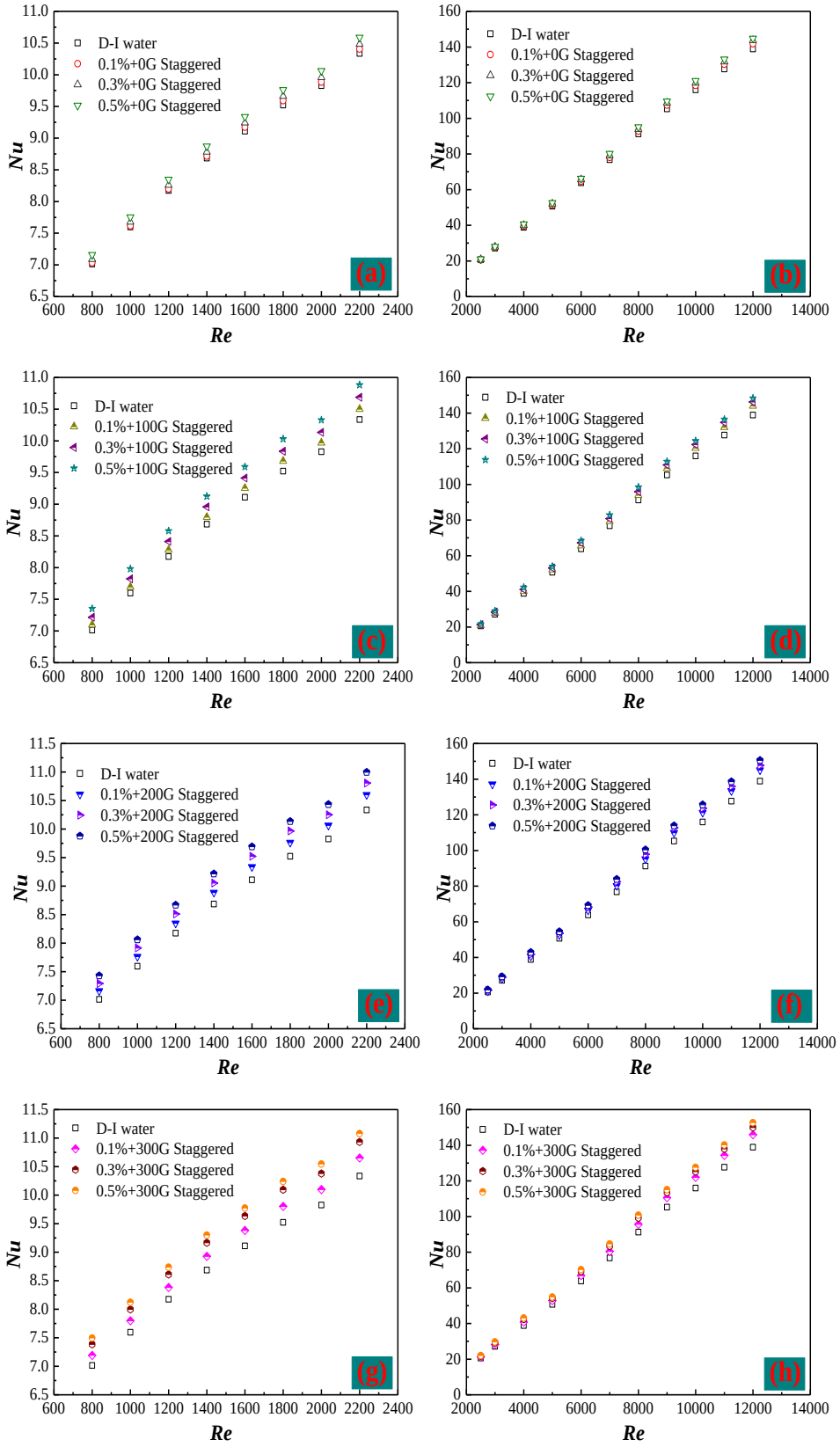

Fig. 8. Effects of nanoparticle mass fractions on Nusselt numbers of corrugated tube with two-side staggered electromagnets. (a) 0G+laminar flow, (b) 0G+turbulent flow, (c) 100G+laminar flow, (d) 100G+turbulent flow, (e) 200G+laminar flow, (f) 200G+turbulent flow,(g) 300G+laminar flow, (h) 300G+turbulent flow

In a word, Nusselt number increases with the mass fraction of nanoparticle, and it shows a larger enhancement ratio under turbulent flow, high magnetic induction intensity and two-side staggered electromagnets than that under laminar flow, low magnetic induction intensity and one-side electromagnets.

3.2.1.2 Effect of magnetic induction intensity

Fig. 9 introduces the effects of magnetic induction intensity on Nusselt numbers of smooth tube with one-side electromagnets. For nanofluids with ω=0.1% in laminar flow, it can be found that Nusselt number of nanofluids under B=0 G, 100 G, 200 G and 300 G can be improved by 2.5%, 2.8%, 3.6%, 4.6% at best compared with water respectively. For nanofluids with ω=0.1% in turbulent flow, it is obtained that Nusselt number of nanofluids under B=0 G, 100 G, 200 G and 300 G can be improved by 6.2%, 6.7%, 8.3%, 9.4% at best compared with water respectively. For nanofluids with ω=0.3% in laminar flow, it can be found that Nusselt number of nanofluids under B=0 G, 100 G, 200 G and 300 G can be improved by 3.3%, 4.2%, 6.3%, 7.7% at best compared with water respectively. For nanofluids with ω=0.3% in turbulent flow, it is obtained that Nusselt number of nanofluids under B=0 G, 100 G, 200 G and 300 G can be improved by 7.6%, 9.0%, 11.3%, 13.2% at best compared with water respectively. For nanofluids with ω=0.5% in laminar flow, it can be found that Nusselt number of nanofluids under B=0 G, 100 G, 200 G and 300 G can be improved by 4.1%, 6.1%, 8.0%, 9.2% at best compared with water respectively. For nanofluids with ω=0.5% in turbulent flow, it is obtained that Nusselt number of nanofluids under B=0 G, 100 G, 200 G and 300 G can be improved by 8.5%, 11.0%, 13.5%, 15.7% at most compared with water respectively. From above analysis, the conclusions we can

get are that Nusselt number increases with the magnetic induction intensity, and the enhancement ration is more sensitive to high nanoparticle mass fraction and turbulence. Nanoparticles can move towards the tube wall under the influence of magnetic field, which not only destroys the laminar boundary layer but also makes nanoparticles concentration higher near the tube wall. Due to the change of

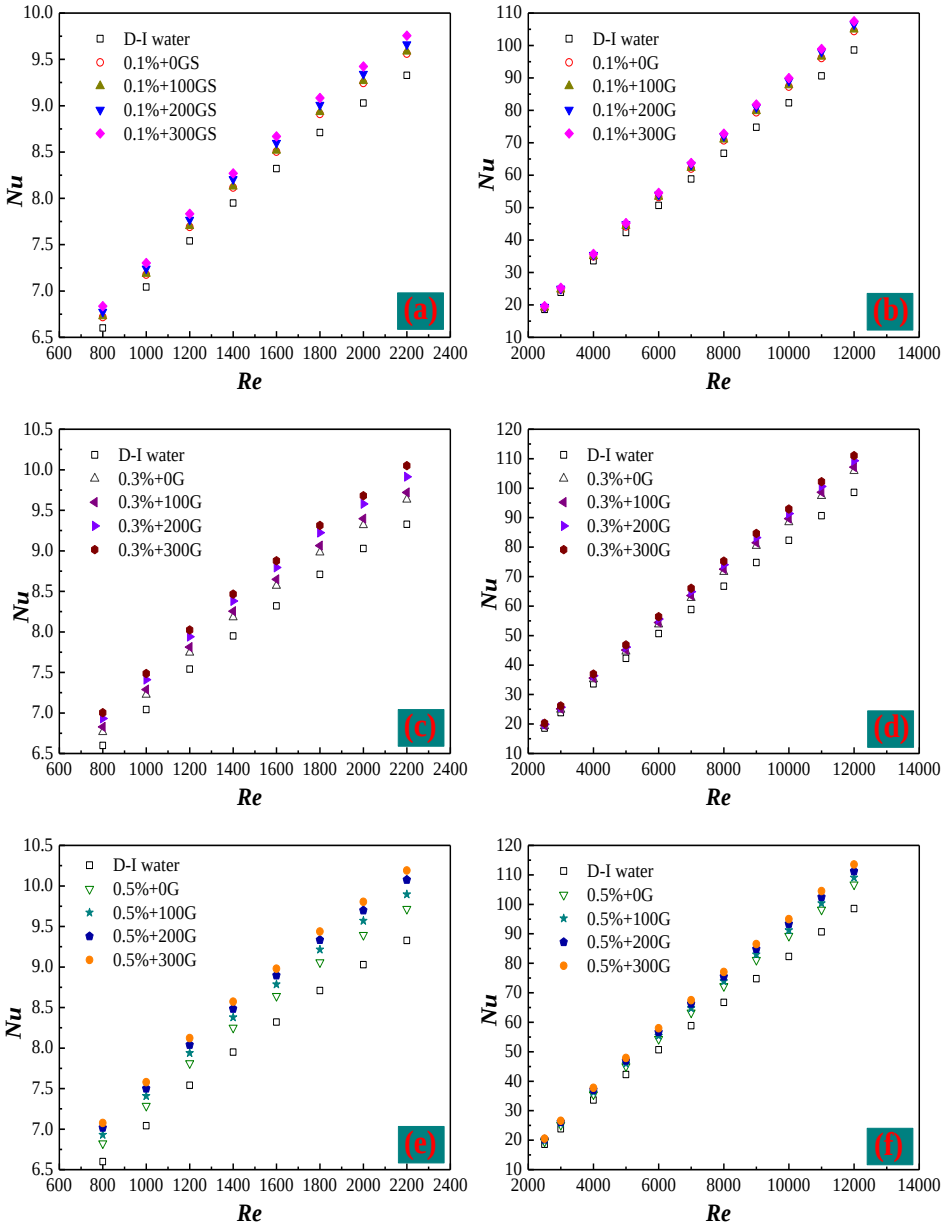

Fig. 9. Effects of magnetic induction intensity on Nusselt numbers of smooth tube with one-side electromagnets. (a) 0.1%+laminar flow, (b) 0.1%+turbulent flow, (c) 0.3%+laminar flow, (d) 0.3%+turbulent flow, (e) 0.5%+laminar flow, (f) 0.5%+turbulent flow

nanoparticle migration, the higher nanoparticle concentration near the tube wall can lead to a higher local thermal conduction and can intensify the Brownian motion of nanoparticles. Besides, the nanoparticle aggregation near the tube wall caused by the magnetic field not only enhances the turbulence of nanofluids but also destroys the laminar boundary layer, and lastly improves the heat transfer.

Fig. 10 presents the effects of magnetic induction intensity on Nusselt numbers of smooth tube with two-side staggered electromagnets. For nanofluids with ω=0.1% in laminar flow, it can be found that Nusselt number of nanofluids under B=0 G, 100 G, 200 G and 300 G can be improved by 2.5%, 3.4%, 4.3%, 5.4% at best compared with water respectively. For nanofluids with ω=0.1% in turbulent flow, it is obtained that Nusselt number of nanofluids under B=0 G, 100 G, 200 G and 300 G can be improved by 6.2%, 7.9%, 9.2%, 10.3% at best compared with water respectively. For nanofluids with ω=0.3% in laminar flow, it can be found that Nusselt number of nanofluids under B=0 G, 100 G, 200 G and 300 G can be improved by 3.3%, 5.6%, 7.2%, 8.8% at best compared with water respectively. For nanofluids with ω=0.3% in turbulent flow, it is obtained that Nusselt number of nanofluids under B=0 G, 100 G, 200 G and 300 G can be improved by 7.6%, 10.4%, 12.6%, 14.7% at best compared with water respectively. For nanofluids with ω=0.5% in laminar flow, it can be found that Nusselt number of nanofluids under B=0 G, 100 G, 200 G and 300 G can be improved by 4.1%, 7.7%, 8.9%, 10.1% at best compared with water respectively. For nanofluids with ω=0.5% in turbulent flow, it is obtained that Nusselt number of nanofluids under B=0 G, 100 G, 200 G and 300 G can be improved by 8.5%, 12.9%, 15.4%, 17.6% at

best compared with that of water.

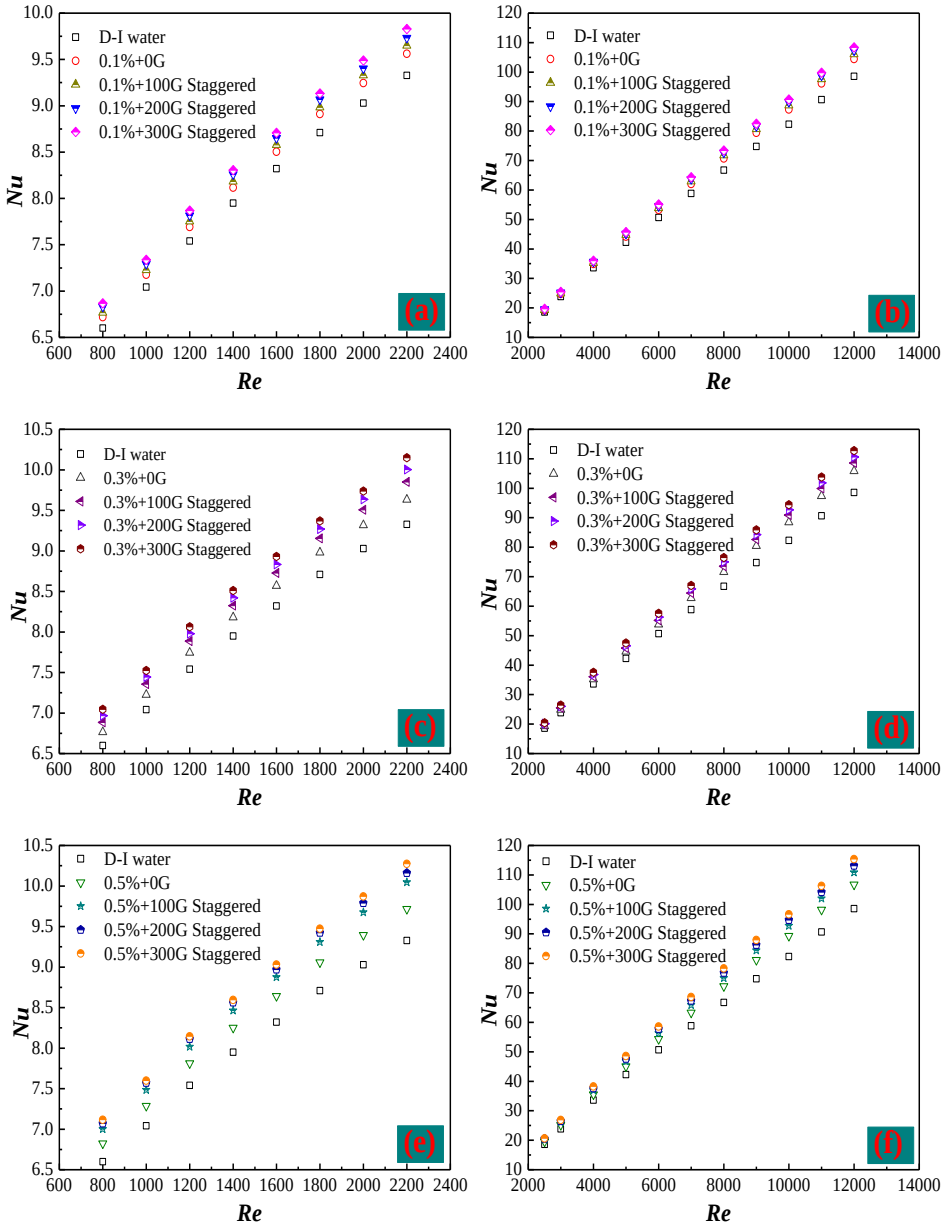

Fig. 10 Effects of magnetic induction intensity on Nusselt numbers of smooth tube with two-side staggered electromagnets. (a) 0.1%+laminar flow, (b) 0.1%+turbulent flow, (c) 0.3%+laminar flow, (d) 0.3%+turbulent flow, (e) 0.5%+laminar flow, (f) 0.5%+turbulent flow

Fig. 11 presents the effects of magnetic induction intensity on Nusselt numbers of corrugated tube with one-side electromagnets. For nanofluids with ω=0.1% in laminar flow, it can be found that Nusselt number of nanofluids under B=0 G, 100 G, 200 G and 300 G can be improved by 0.7%, 0.9%, 2.0%, 2.7% at best compared with

water respectively. For nanofluids with ω=0.1% in turbulent flow, it is obtained that Nusselt number of nanofluids under B=0 G, 100 G, 200 G and 300 G can be improved by 2.2%, 2.8%, 4.0%, 4.8% at best compared with water respectively. For nanofluids with ω=0.3% in laminar flow, it can be found that Nusselt number of nanofluids under B=0 G, 100 G, 200 G and 300 G can be improved by 1.5%, 2.5%, 4.3%, 5.3%

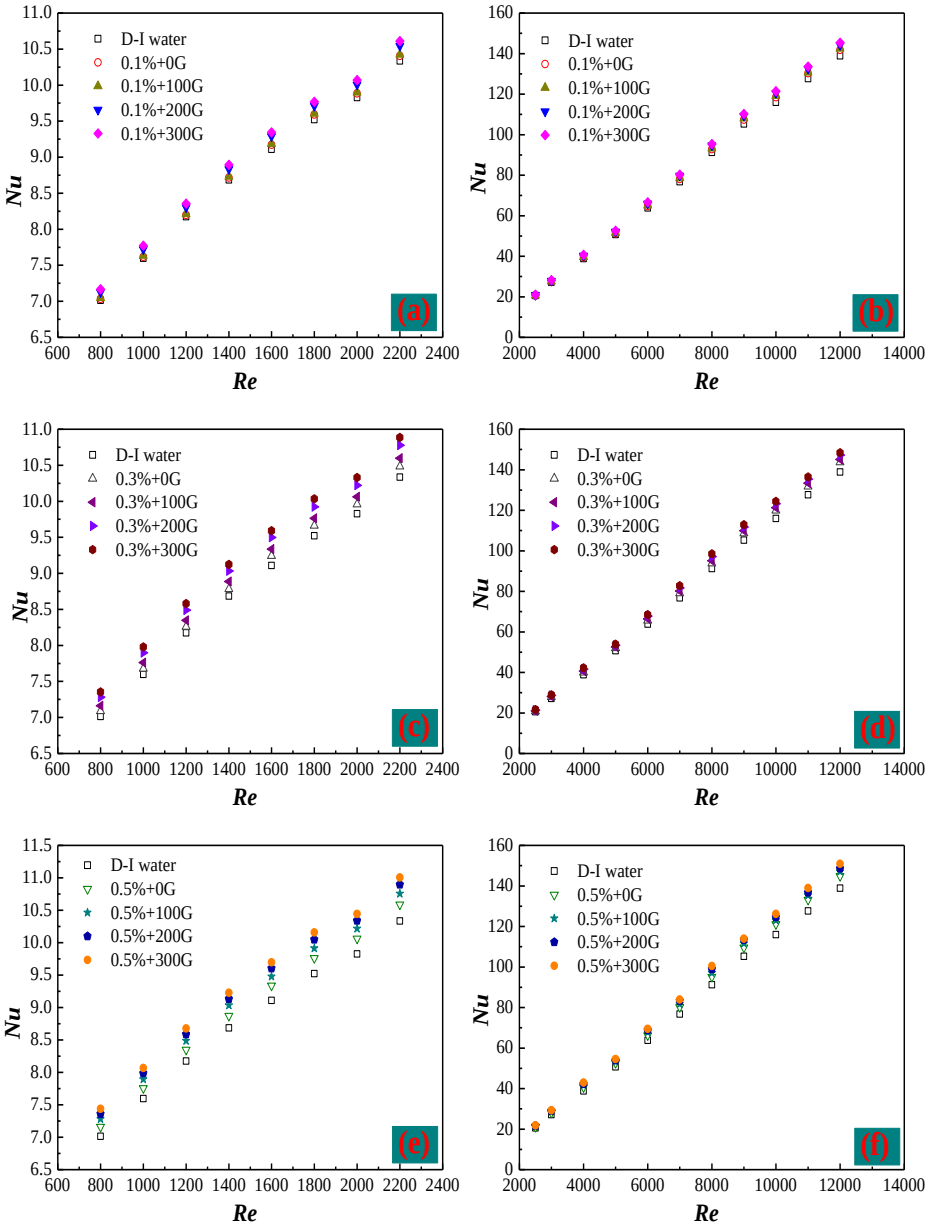

Fig. 11 Effects of magnetic induction intensity on Nusselt numbers of corrugated tube with one-side electromagnets. (a) 0.1%+laminar flow, (b) 0.1%+turbulent flow, (c) 0.3%+laminar flow, (d) 0.3%+turbulent flow, (e) 0.5%+laminar flow, (f) 0.5%+turbulent flow

at best compared with water respectively. For nanofluids with ω=0.3% in turbulent flow, it is obtained that Nusselt number of nanofluids under B=0 G, 100 G, 200 G and 300 G can be improved by 3.4%, 4.6%, 6.3%, 7.3% at best compared with water respectively. For nanofluids with ω=0.5% in laminar flow, it can be found that Nusselt number of nanofluids under B=0 G, 100 G, 200 G and 300 G can be improved by 2.4%, 4.1%, 5.4%, 6.5% at best compared with water respectively. For nanofluids with ω=0.5% in turbulent flow, it is obtained that Nusselt number of nanofluids under B=0 G, 100 G, 200 G and 300 G can be improved by 4.4%, 6.2%, 7.5%, 8.9% at best compared with that of water.

Fig. 12 shows the effects of magnetic induction intensity on Nusselt numbers of corrugated tube with two-side staggered electromagnets. For nanofluids with ω=0.1% in laminar flow, it can be found that Nusselt number of nanofluids under B=0 G, 100 G, 200 G and 300 G can be improved by 0.7%, 1.6%, 2.6%, 3.1% at best compared with water respectively. For nanofluids with ω=0.1% in turbulent flow, it is obtained that Nusselt number of nanofluids under B=0 G, 100 G, 200 G and 300 G can be improved by 2.2%, 3.8%, 4.6%, 5.2% at best compared with water respectively. For nanofluids with ω=0.3% in laminar flow, it can be found that Nusselt number of nanofluids under B=0 G, 100 G, 200 G and 300 G can be improved by 1.5%, 3.4%, 4.6%, 5.8% at best compared with water respectively. For nanofluids with ω=0.3% in turbulent flow, it is obtained that Nusselt number of nanofluids under B=0 G, 100 G, 200 G and 300 G can be improved by 3.4%, 5.6%, 6.7%, 8.1% at best compared with water respectively. For nanofluids with ω=0.5% in laminar flow, it is obtained that

Nusselt number of nanofluids under B=0 G, 100 G, 200 G and 300 G can be improved by 2.4%, 5.3%, 6.4%, 7.2% at best compared with water respectively. For nanofluids with ω=0.5% in turbulent flow, it can be found that Nusselt number of nanofluids under B= 0 G, 100 G, 200 G and 300 G can be improved by 4.4%, 7.3%, 8.6%, 10.0% at best compared with that of water.

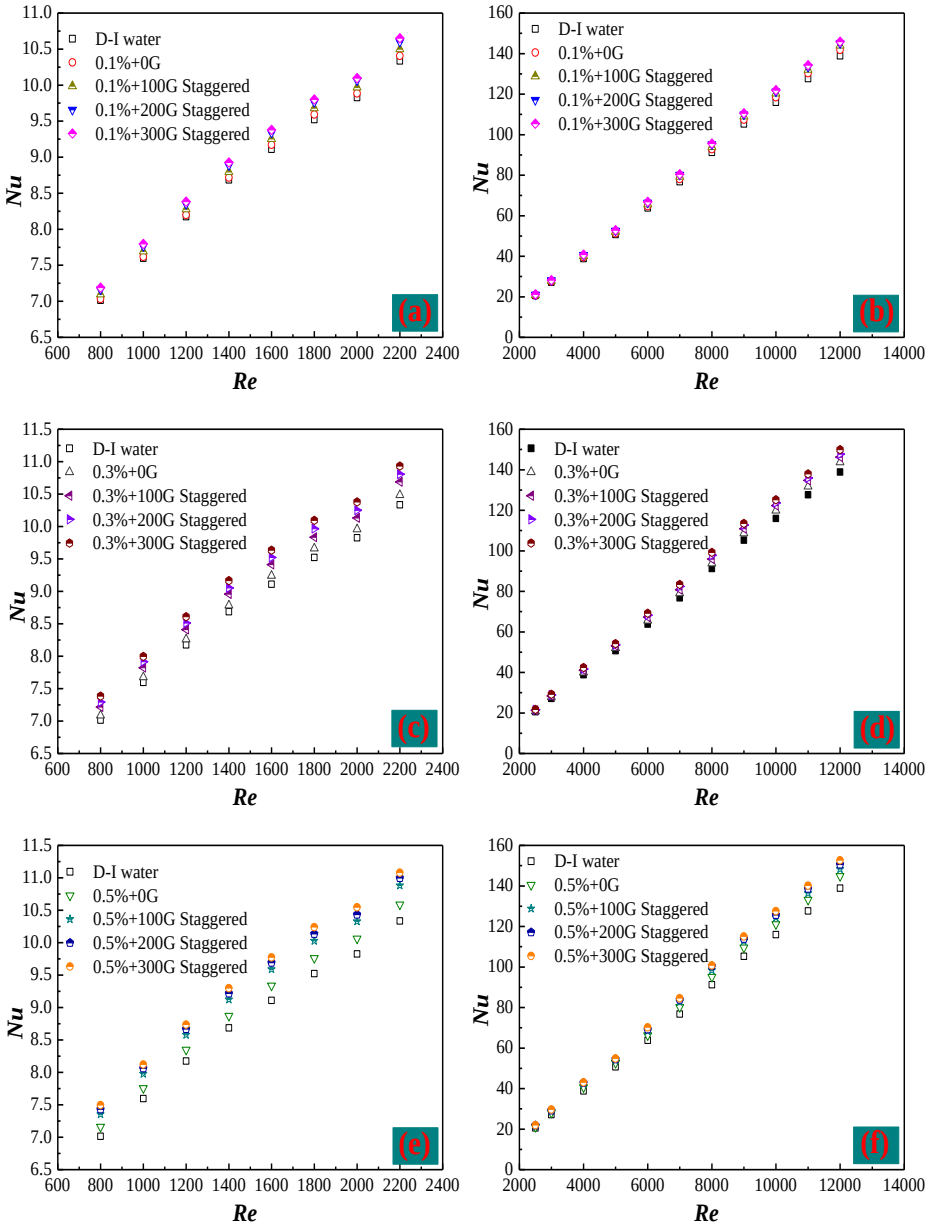

Fig. 12 Effects of magnetic induction intensity on Nusselt numbers of corrugated tube with two-side staggered electromagnets. (a) 0.1%+laminar flow, (b) 0.1%+turbulent flow, (c) 0.3%+laminar flow, (d) 0.3%+turbulent flow, (e) 0.5%+laminar flow, (f) 0.5%+turbulent flow

In a word, Nusselt number increases with the magnetic induction intensity, and the enhancement ratio is much more sensitive to two-side staggered electromagnets instead of one-side electromagnets, turbulent flow instead of laminar flow, and high nanoparticle concentration instead of low nanoparticle concentration.

3.2.1.3 Effect of electromagnet arrangement mode

Fig. 13 shows the effects of two kinds of electromagnet arrangement modes on Nusselt numbers. For the smooth tube, compared with one-side electromagnets, Nusselt number of nanofluids with two-side staggered electromagnets can be improved by 1.5% in laminar flow and 2.0% in turbulent flow at most. For the corrugated tube, compared with one-side electromagnets, Nusselt number of

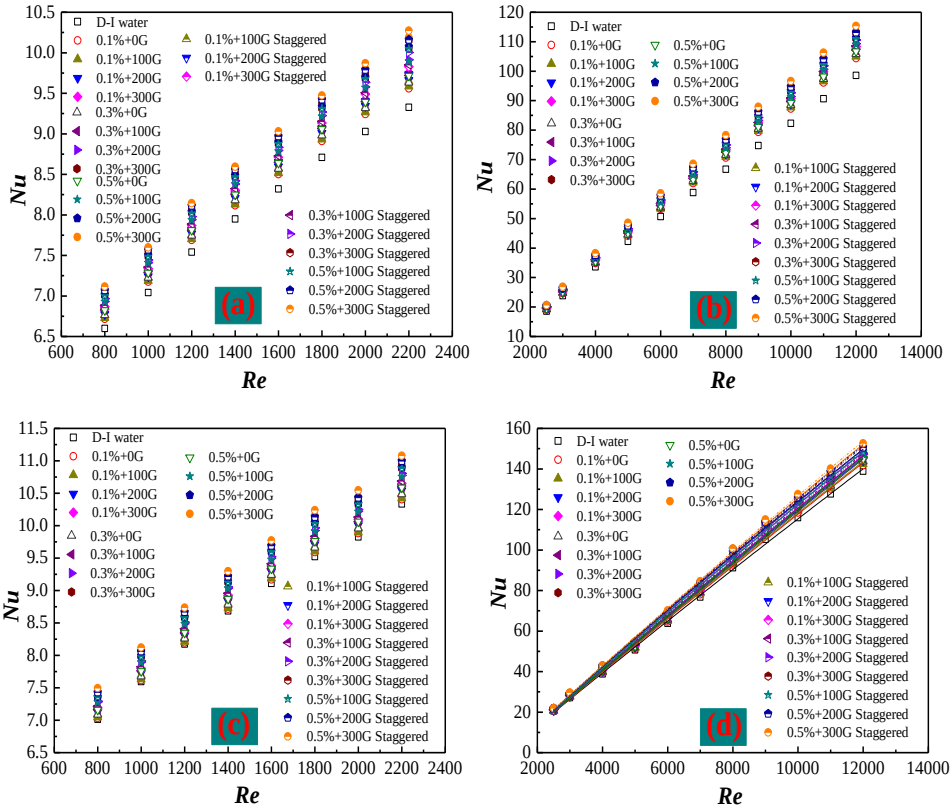

Fig. 13 Effects of two kinds of electromagnet arrangement modes on Nusselt numbers, Smooth tube: (a) laminar flow, (b) turbulent flow, Corrugated tube: (c) laminar flow, (d) turbulent flow

nanofluids with two-side staggered electromagnets can be improved by 1.2% and 1.5% at best in laminar flow and turbulent flow respectively. For two-side staggered electromagnets, nanoparticles can move toward top and bottom tube wall, which not only destroy the two-side laminar boundary layer but also disturb the flow of nanofluids. The increase of turbulence can improve the rate of heat transfer. However, for the one-side electromagnets, nanoparticles move toward one side of tube wall, and only destroy the one side laminar boundary layer. Hence, arrangement mode of two-side staggered electromagnets is better than that of one-side electromagnets.

Because the flow state of working fluid in the corrugated tube is usually turbulent flow in industry, a fitting formula (16) for one-side and two-side staggered arrangement is established based on the experimental data to present the relationship between Reynolds number and Nusselt number in turbulent flow. The lines in Fig. 13 (d) represent the fitting formula curves, and the points are experimental results. The constants of the fitting formula (16) are shown in Table 2. It can be discovered that the fitting formula curves are highly consistent with the experimental data.

$$Nu=\mathrm{A}+\mathrm{B}Re+\mathrm{C}Re^2 \tag{16}$$

By comparing the Nusselt number of smooth tube with that of corrugated tube in Fig. 14, it presents that the Nusselt number of nanofluids in the corrugated tube can be increased by 9.1% and 35.8% at best in laminar flow and turbulent flow respectively, which not only indicates that the enhancement ratio of Nusselt number is larger in turbulent flow but also shows the advantage of the corrugated tube. The influence of enhancement ratio of resistance which is due to the increasing nanoparticle

Table 2 Constants in formula (16)

Mass fraction	Arrangement model	Magnetic induction intensity	A	B	C
0.0%	One-side	/	-13.04476	0.01325	-4.08E-08
0.1%	One-side	0G	-13.39133	0.01343	-3.21E-08
		100G	-13.71748	0.01359	-3.88E-08
		200G	-14.13361	0.01385	-4.62E-08
		300G	-14.12784	0.01394	-4.51E-08
	Two-side staggered	100G	-13.64609	0.01363	-3.23E-08
		200G	-14.03535	0.01389	-4.35E-08
		300G	-14.09995	0.01395	-4.17E-08
0.3%	One-side	0G	-13.49536	0.01358	-3.17E-08
		100G	-14.04813	0.0139	-4.40E-08
		200G	-14.70264	0.01433	-6.12E-08
		300G	-15.18852	0.01466	-7.68E-08
	Two-side staggered	100G	-14.11597	0.01402	-4.50E-08
		200G	-15.26363	0.0146	-7.63E-08
		300G	-15.07561	0.01464	-6.57E-08
0.5%	One-side	0G	-14.09582	0.01391	-4.66E-08
		100G	-14.66665	0.01432	-6.10E-08
		200G	-15.80366	0.01491	-9.23E-08
		300G	-15.33177	0.0148	-6.99E-08
	Two-side staggered	100G	-15.24921	0.01466	-7.73E-08
		200G	-15.27511	0.01477	-7.08E-08
		300G	-15.18014	0.01477	-5.77E-08

concentration and the roughened surface of the corrugated tube is relatively large in laminar flow, which causes a small increase in Nusselt number. However, the higher turbulence caused by the rough surface of corrugated tube can accelerate the heat transfer rate and cause a larger enhancement ratio of Nusselt number than that of resistance. Hence, enhancement ratio of Nusselt number in turbulent flow is larger than that in laminar flow.

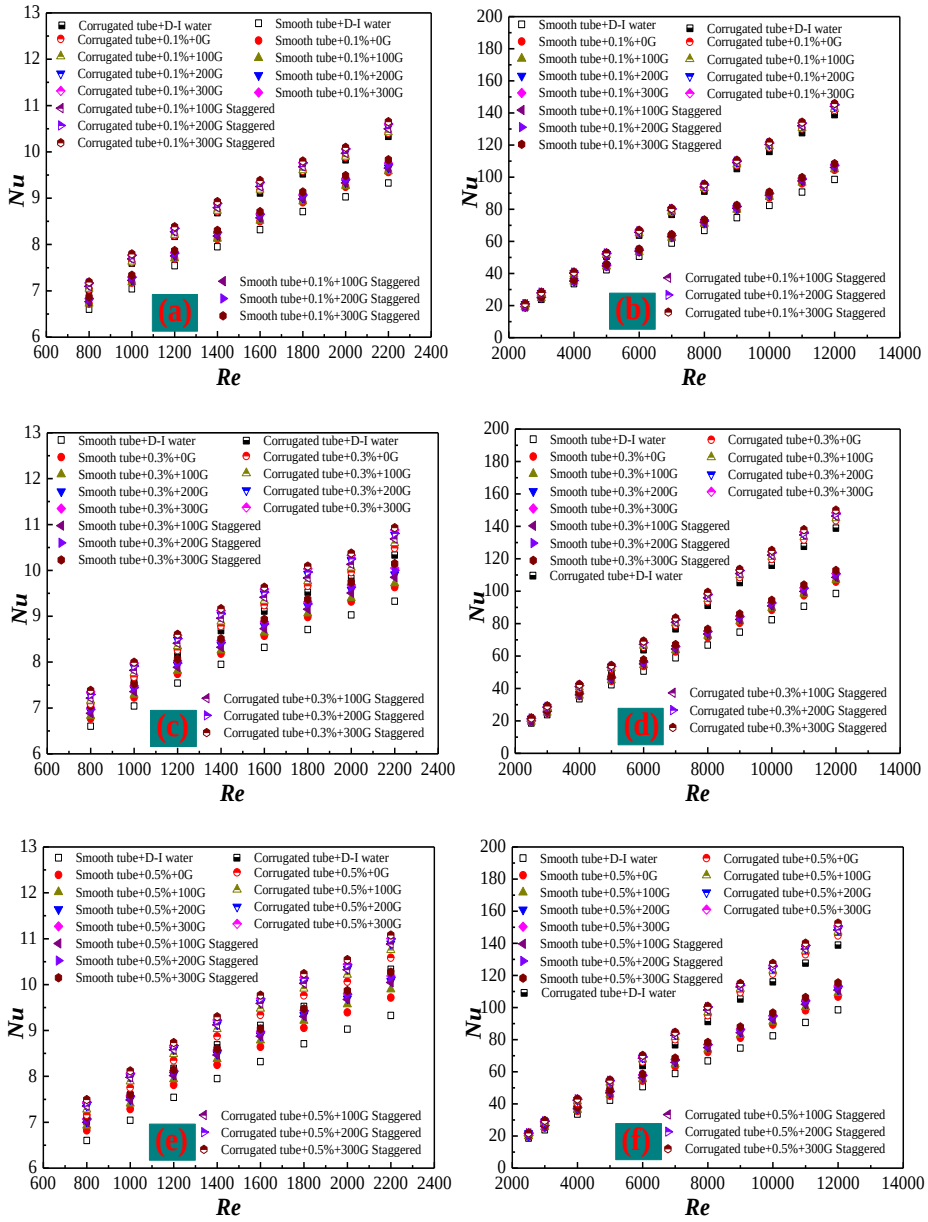

Fig. 14 Nusselt number comparison between smooth tube and corrugated tube, ω=0.1%: (a) laminar flow, (b) turbulent flow, ω=0.3%: (c) laminar flow, (d) turbulent flow, ω=0.5%: (e) laminar flow, (f) turbulent flow

3.2.2 Resistance coefficient

Adding nanoparticles into base fluid and the rough surface not only improve the heat transfer but also cause an increase in resistance coefficient. Fig. 15 presents the effects of two kinds of electromagnet arrangement modes on resistance coefficients. For the smooth tube, compared with one-side electromagnets, resistance coefficient of nanofluids with two-side staggered electromagnets is increased by 0.4% in laminar

flow and 0.5% in turbulent flow at most. For the corrugated tube, compared with one-side electromagnets, resistance coefficient of nanofluids with two-side staggered electromagnets is increased by 0.5% in laminar flow and 0.7% in turbulent flow at most. All of these indicate that resistance coefficient is more sensitive to turbulent flow and two-side staggered electromagnets. It is because the larger turbulence caused by turbulent flow plays a major role in enhancement of resistance. Moreover, the movement of nanoparticles toward two directions intensifies the augment of resistance coefficient. It can be also found that that the enhancement ratio of resistance coefficient is much smaller than that of Nusselt number.

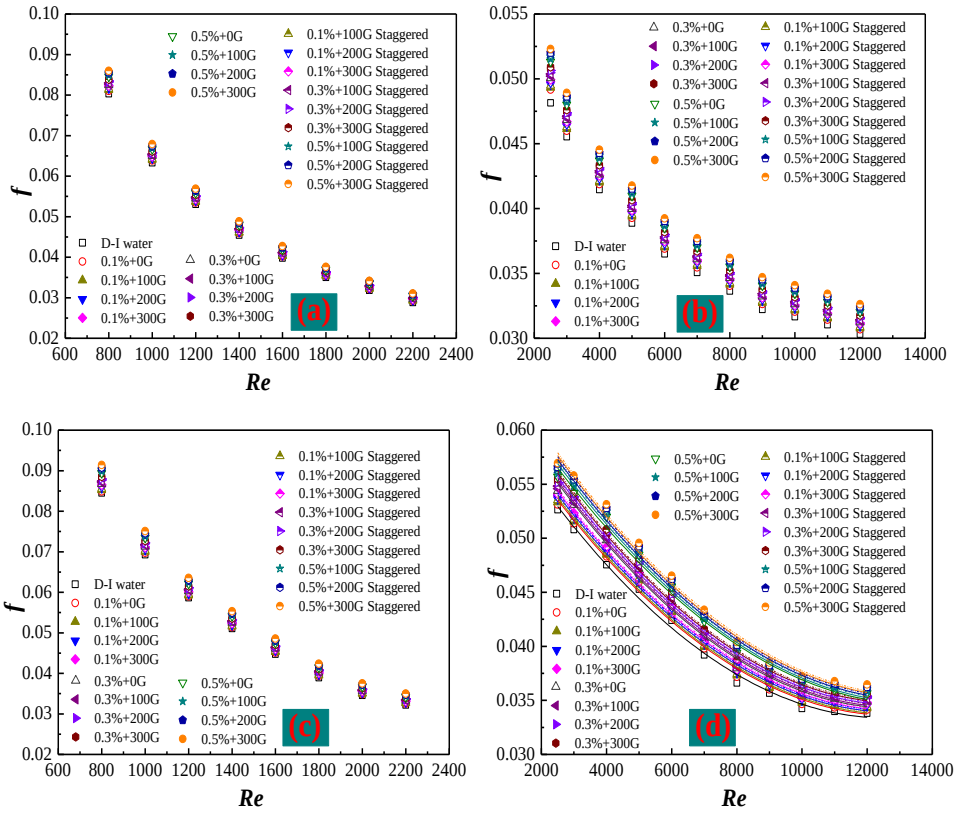

Fig. 15. Effects of two kinds of electromagnet arrangement modes on resistance coefficients, Smooth tube: (a) laminar flow, (b) turbulent flow, Corrugated tube: (c) laminar flow, (d) turbulent flow

The relationship between Reynolds number and resistance coefficient is presented in formula (17), and relevant constants are given in Table (3). It can be found from

Fig. 15. (d) that the fitting formula curves agree well with the experimental results.

$$f=A+BRe+CRe^2 \quad (17)$$

Table 3 Constants in formula (17)

Mass fraction	Arrangement model	Magnetic induction intensity	A	B	C
0.0%	One-side	/	0.06388	-4.86E-06	1.93E-10
0.1%	One-side	0G	0.06436	-4.80E-06	1.87E-10
		100G	0.06459	-4.81E-06	1.88E-10
		200G	0.06496	-4.84E-06	1.89E-10
		300G	0.06532	-4.87E-06	1.90E-10
	Two-side staggered	100G	0.06483	-4.83E-06	1.88E-10
		200G	0.0652	-4.86E-06	1.89E-10
		300G	0.06556	-4.89E-06	1.91E-10
0.3%	One-side	0G	0.06638	-5.00E-06	1.94E-10
		100G	0.06664	-5.01E-06	1.95E-10
		200G	0.06705	-5.05E-06	1.96E-10
		300G	0.06746	-5.08E-06	1.97E-10
	Two-side staggered	100G	0.0669	-5.03E-06	1.96E-10
		200G	0.06732	-5.07E-06	1.97E-10
		300G	0.06773	-5.10E-06	1.98E-10
0.5%	One-side	0G	0.06749	-4.84E-06	1.78E-10
		100G	0.06805	-4.92E-06	1.82E-10
		200G	0.06851	-4.95E-06	1.83E-10
		300G	0.06896	-4.98E-06	1.84E-10
	Two-side staggered	100G	0.06836	-4.94E-06	1.83E-10
		200G	0.06882	-4.97E-06	1.84E-10
		300G	0.06922	-4.99E-06	1.84E-10

Fig. 16 gives the comparison between smooth tube and corrugated tube on resistance coefficients. It can be found that nanofluids with ω=0.1% in corrugated tube can increase the resistance coefficients by 12.6% and 17.3% at best in laminar flow and turbulent flow respectively. Nanofluids with ω=0.3% in corrugated tube can increase the resistance coefficients by 13.1% and 18.4% at best in laminar flow and turbulent flow respectively. Nanofluids with ω=0.5% in corrugated tube can increase

the resistance coefficients by 13.7% and 19.3% at best in laminar flow and turbulent flow respectively. The roughened surface of corrugated tube causes an increase in resistance coefficient.

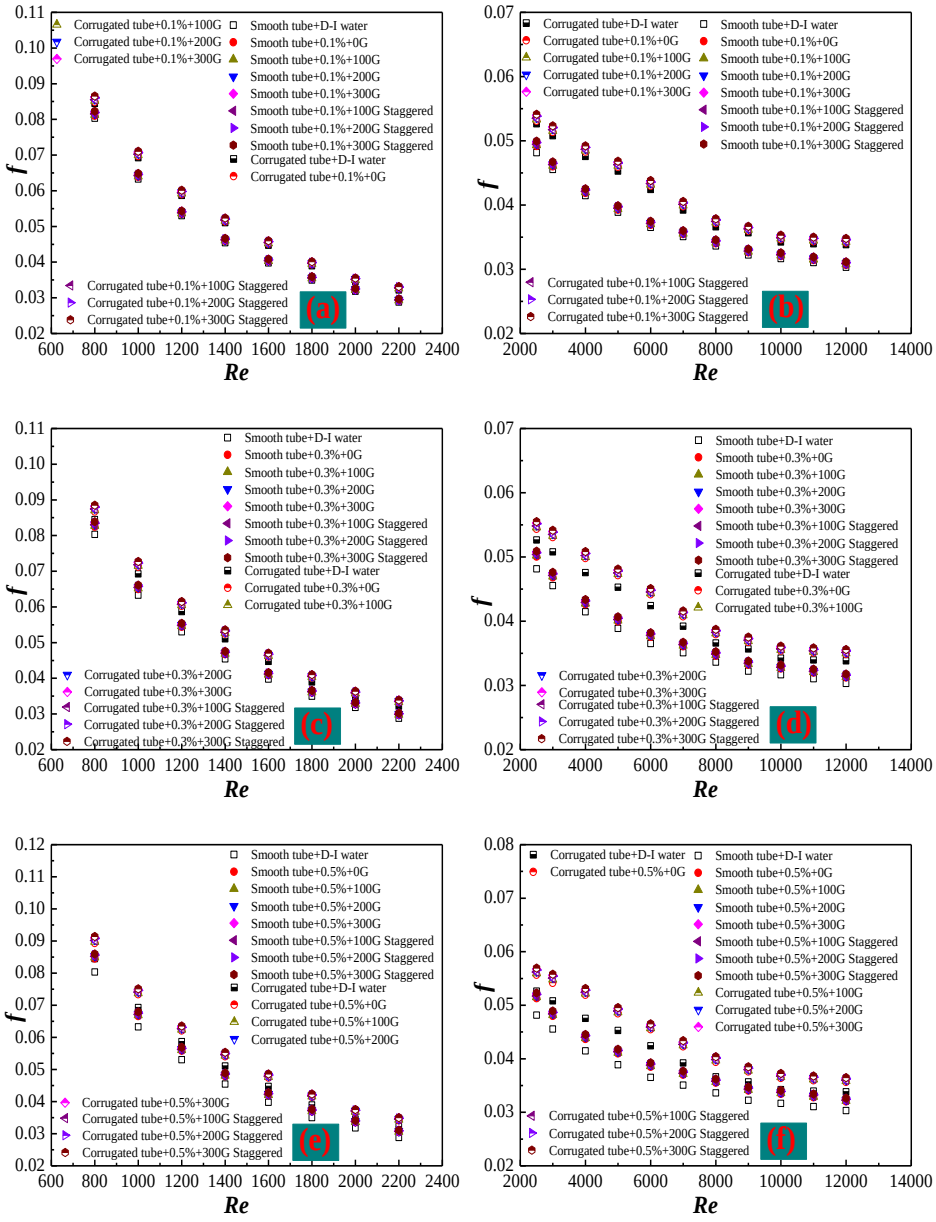

Fig. 16 Comparison between smooth tube and corrugated tube on resistance coefficients, ω=0.1%: (a) laminar flow, (b) turbulent flow, ω=0.3%: (c) laminar flow, (d) turbulent flow, ω=0.5%: (e) laminar flow, (f) turbulent flow.

3.2.3 Pressure drop

Fig. 17 shows the pressure drop in laminar and turbulent flow. For the smooth tube, compared with one-side electromagnets, pressure drop of nanofluids with

two-side staggered electromagnets is increased by 0.4% in laminar flow and 0.5% in turbulent flow at most. For the corrugated tube, compared with one-side electromagnets, pressure drop of nanofluids with two-side staggered electromagnets can be increased by 0.5% and 0.7% at best in laminar flow and turbulent flow respectively.

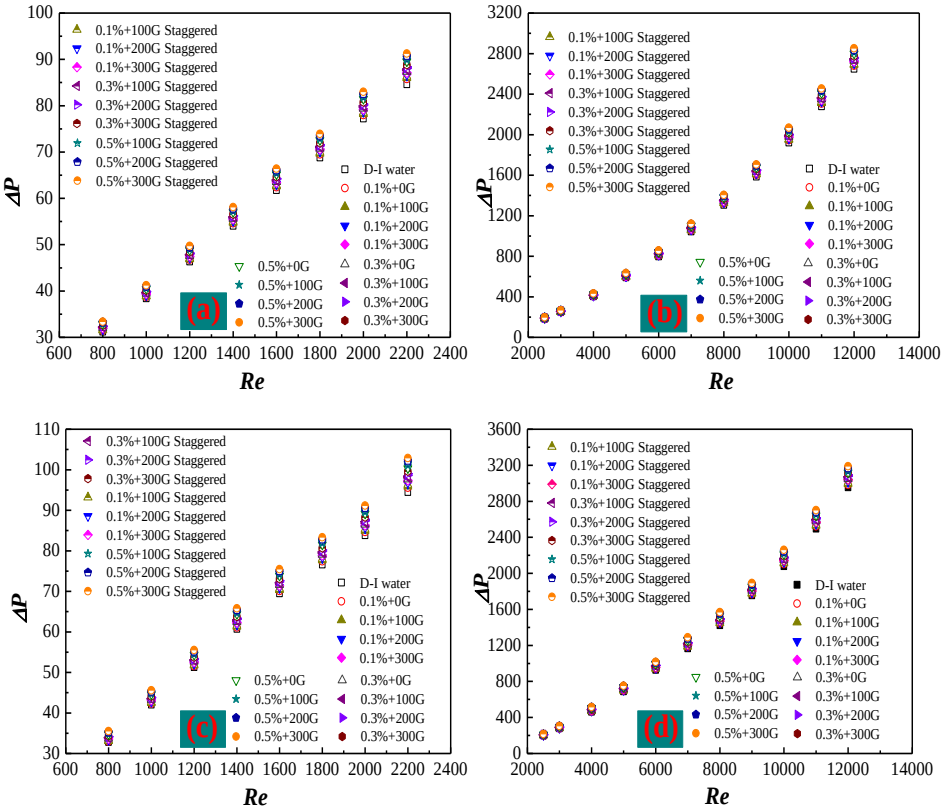

Fig. 17. Pressure drop under laminar and turbulent flow. Smooth tube: (a) laminar flow, (b) turbulent flow, Corrugated tube: (c) laminar flow, (d) turbulent flow

Fig. 18 presents the comparison between smooth tube and corrugated tube on pressure drop. It can be found that nanofluids with ω=0.1% in corrugated tube can increase the pressure drop by 12.7% and 17.3% at best in laminar flow and turbulent flow respectively. Nanofluids with ω=0.3% in corrugated tube can increase the pressure drop by 13.1% and 18.4% at best in laminar flow and turbulent flow respectively. Nanofluids with ω=0.5% in corrugated tube can increase the pressure

drop by 13.7% and 19.3% at best in laminar flow and turbulent flow respectively.

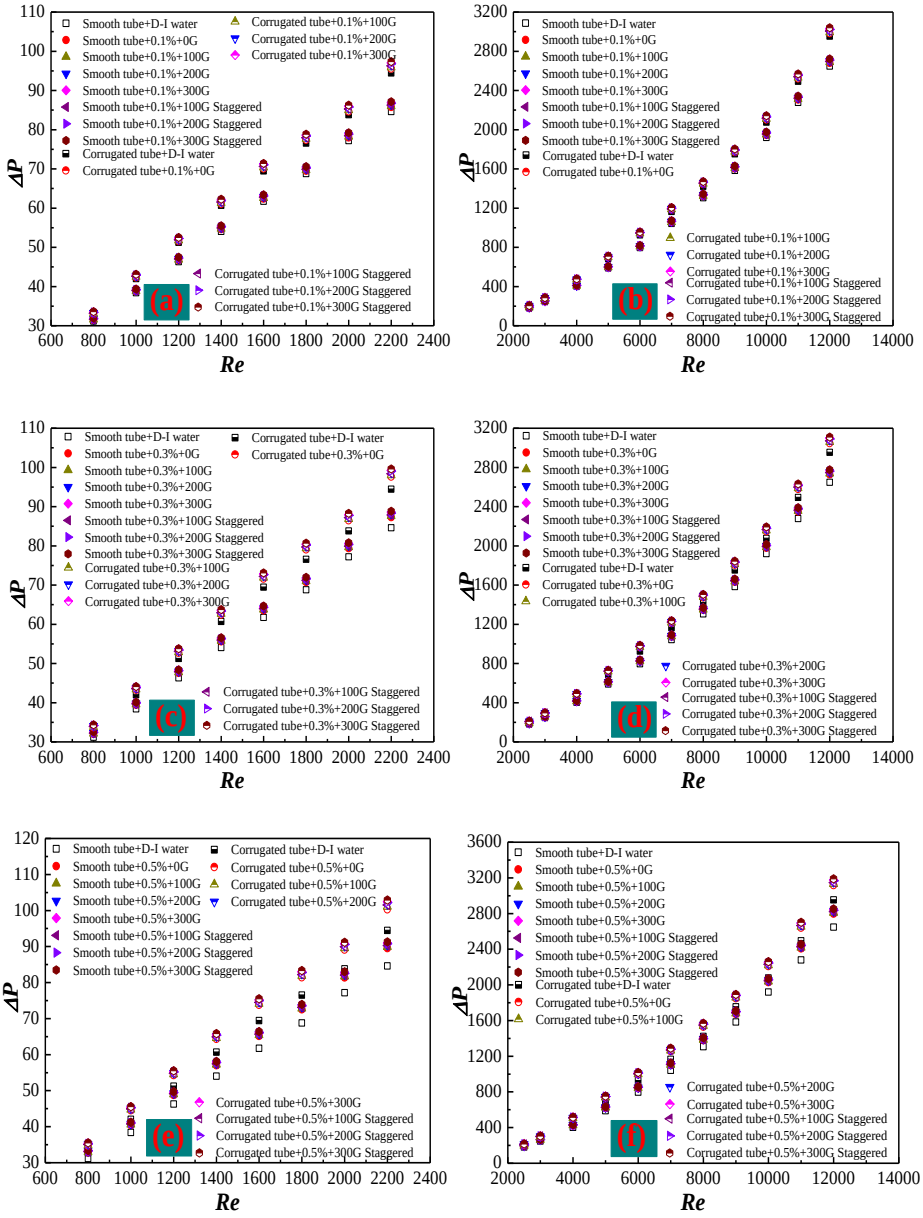

Fig. 18 Comparison between smooth tube and corrugated tube on pressure drop, ω=0.1%: (a) laminar flow, (b) turbulent flow, ω=0.3%: (c) laminar flow, (d) turbulent flow, ω=0.5%: (e) laminar flow, (f) turbulent flow.

3.2.4 Comprehensive evaluation index

Fig. 19 presents the comprehensive evaluation index which is used to evaluate the thermo-hydraulic performance. It is obtained that with the increasing Reynolds number, the comprehensive evaluation index increases at first, and then decreases. A critical Reynolds number which indicates the maximum of comprehensive evaluation

index can be also found. The critical Reynold number is *Re*=9000 for the smooth tube, and it is *Re*=10000 for the corrugated tube. The reason is that the influences of magnetic induction intensity, nanoparticle mass fraction play a major role on the heat transfer enhancement ratio before the critical Reynolds number. However, after the critical Reynolds number, the influences of nanoparticle mass fraction, magnetic induction intensity play a major role on the flow resistance enhancement ratio and cause a decline in the comprehensive evaluation index. The reason for the difference between the critical Reynolds numbers of smooth and corrugated tube is that the rough surface of corrugated has a certain effect on the enhancement ratio of heat transfer and delays the appearance of the critical Reynolds number.

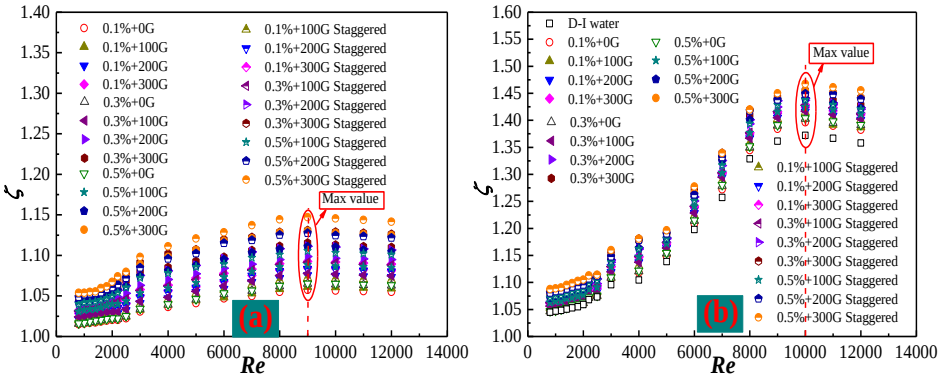

Fig. 19. Comprehensive evaluation index for the thermo-hydraulic performance, (a) Smooth tube, (b) Corrugated tube

Fig. 20 shows the comparison between smooth tube and corrugated tube on comprehensive evaluation index for the thermo-hydraulic performance. In addition to the difference of the critical Reynolds number, it is also obtained that the comprehensive evaluation index of corrugated tube can be improved by 32.3%, 31.9% and 31.8% at best for nanofluids with ω=0.1%, 0.3% and 0.5% compared that of smooth tube respectively, which indicates that the enhancement ratio of resistance

coefficient caused by corrugated tube is much smaller than that of heat transfer.

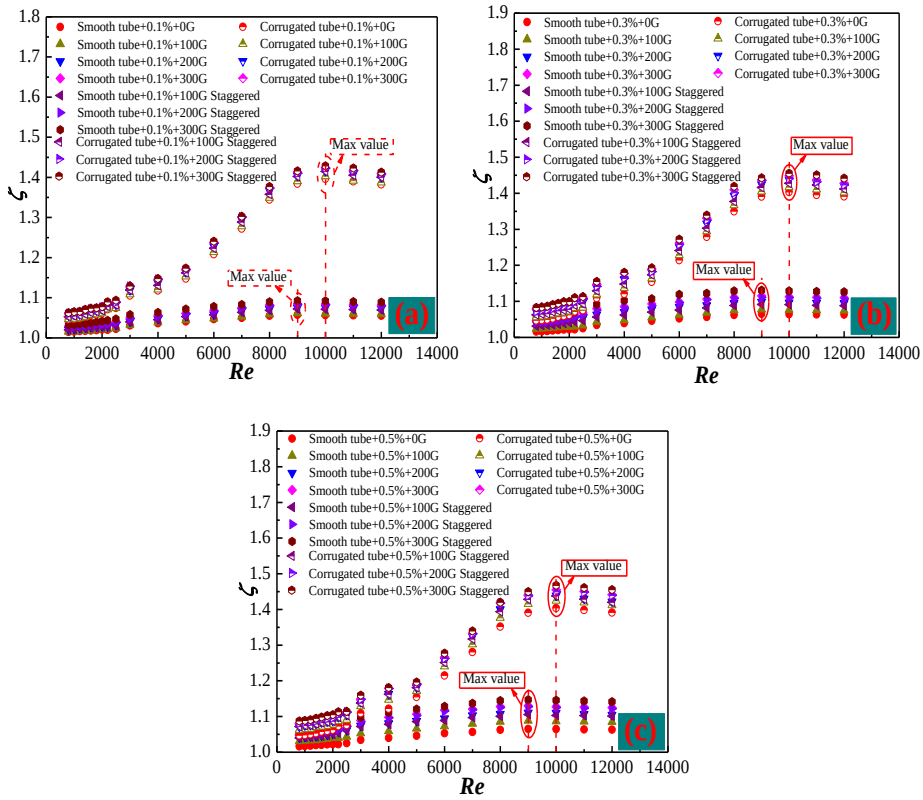

Fig. 20 Comparison between smooth tube and corrugated tube on comprehensive evaluation index for the thermo-hydraulic performance, (a) ω=0.1%, (b) ω=0.3%, (c) ω=0.5%.

4 Conclusions

Flow resistance characteristics and heat transfer enhancement in a corrugated tube full of Fe_3O_4-water nanofluids under various magnetic fields are experimentally investigated. Some main conclusions can be summarized as follows:

(1) Nusselt number increases with magnetic induction intensity and mass fraction of nanoparticle. Nusselt numbers of smooth and corrugated tube filled with nanofluids under the magnetic field can be improved by 17.6% and 10.0% compared with that of water at best respectively.

(2) Heat transfer enhancement ratio is more sensitive to two-side staggered electromagnets than one-side electromagnets. Nusselt number of nanofluids with

two-side staggered electromagnets can be improved by 2.0% at best compared with that with one-side electromagnets.

(3) Heat transfer enhancement ratio is more sensitive to corrugated tube than smooth tube. Nusselt numbers of the corrugated tube filled with nanofluids can be improved by 35.8% at best compared with smooth tube.

(4) The coupling of nanofluids, corrugated tube and magnetic field can enhance the heat transfer effectively at a little expense of increasing flow resistance. The enhancement ratios of resistance coefficient and press drop are smaller than that of Nusselt number.

(5) The comprehensive evaluation index increases with Reynolds number at first and then decreases. A critical Reynolds number can be discovered (smooth tube: *Re*=9000, corrugated tube: *Re*=10000) for the highest comprehensive evaluation index. The rough surface of corrugated tube delays the appearance of critical Reynolds number.

Acknowledgements

This work is financially supported by "National Natural Science Foundation of China" (Grant No. 51606214) and "Postgraduate Research & Practice Program of Education & Teaching Reform of CUMT".

References

[1] N.R. Kumar, P. Bhramara, A. Kirubeil, L.S. Sundar, M.K. Singh, A.C. Sousa, Effect of twisted tape inserts on heat transfer, friction factor of Fe_3O_4 nanofluids flow in a double pipe U-bend heat exchanger, Int. Commun. Heat Mass

Transf. 95 (2018) 53-62.

[2] N.R. Kumar, P. Bhramara, B.M. Addis, L.S. Sundar, M.K. Singh, A.C. Sousa, Heat transfer, friction factor and effectiveness analysis of Fe_3O_4/water nanofluid flow in a double pipe heat exchanger with return bend, Int. Commun. Heat Mass Transf. 81 (2017)155-163.

[3] C. Qi, N. Zhao, X. Cui, T. Chen, J. Hu, Effects of half spherical bulges on heat transfer characteristics of CPU cooled by TiO_2-water nanofluids, Int. J. Heat Mass Transf. 123 (2018) 320-330.

[4] C. Qi, J. Hu, M. Liu, L. Guo, Z. Rao, Experimental study on thermo-hydraulic performances of CPU cooled by nanofluids, Energy Convers. Manage. 153 (2017) 557-565.

[5] B. Sun, H. Liu, Flow and heat transfer characteristics of nanofluids in a liquid-cooled CPU heat radiator, Appl. Therm. Eng. 115 (2017) 435-443.

[6] P. Naphon, S. Wiriyasart, Pulsating flow and magnetic field effects on the convective heat transfer of TiO_2-water nanofluids in helically corrugated tube, Int. J. Heat Mass Transf. 125 (2018) 1054-1060.

[7] P. Naphon, S. Wiriyasart, Experimental study on laminar pulsating flow and heat transfer of nanofluids in micro-fins tube with magnetic fields, Int. J. Heat Mass Transf. 118 (2018) 297-303.

[8] M. Sheikholeslami, Solidification of NEPCM under the effect of magnetic field in a porous thermal energy storage enclosure using CuO nanoparticles, J. Mol. Liq. 263 (2018) 303-315.

[9] C. Qi, G. Wang, Y. Yan, S. Mei, T. Luo, Effect of rotating twisted tape on thermo-hydraulic performances of nanofluids in heat-exchanger systems, Energy Convers. Manage. 166 (2018) 744-757.

[10] Y. Hu, Z. Liu, Y. He, Effects of SiO_2 nanoparticles on pool boiling heat transfer characteristics of water based nanofluids in a cylindrical vessel, Powder Technol. 327 (2018) 79-88.

[11] M. Chen, Y. He, X. Wang, Y. Hu, Complementary enhanced solar thermal conversion performance of core-shell nanoparticles, Appl. Energ. 211 (2018) 735-742.

[12] X. Zhou, X. Li, K. Cheng, X. Huai, Numerical study of heat transfer enhancement of nano liquid-metal fluid forced convection in circular tube, ASME J. Heat Transf. 140 (8) (2018) 081901.

[13] C. Qi, Y.L. Wan, C.Y. Li, D.T. Han, Z.H. Rao, Experimental and numerical research on the flow and heat transfer characteristics of TiO_2-water nanofluids in a corrugated tube, Int. J. Heat Mass Transf. 115 (2017) 1072-1084.

[14] H. Han, B. Li, W. Shao, Effect of flow direction for flow and heat transfer characteristics in outward convex asymmetrical corrugated tubes, Int. J. Heat Mass Transf. 92 (2016) 1236-1251.

[15] H.Z. Han, B.X. Li, H. Wu, W. Shao, Multi-objective shape optimization of double pipe heat exchanger with inner corrugated tube using RSM method, Int. J. Therm. Sci. 90 (2015) 173-186.

[16] D. Yang, B. Sun, H. Li, C. Zhang, Y. Liu, Comparative study on the heat transfer

characteristics of nano-refrigerants inside a smooth tube and internal thread tube, Int. J. Heat Mass Transf. 113 (2017) 538-543.

[17] B. Sun, A. Yang, D. Yang, Experimental study on the heat transfer and flow characteristics of nanofluids in the built-in twisted belt external thread tubes, Int. J. Heat Mass Transf. 107 (2017) 712-722.

[18] L.W. Fan, J.Q. Li, Y.Z. Wu, L. Zhang, Z.T. Yu, Pool boiling heat transfer during quenching in carbon nanotube (CNT)-based aqueous nanofluids: Effects of length and diameter of the CNTs, Appl. Therm. Eng. 122 (2017) 555-565.

[19] L.W. Fan, J.Q. Li, D.Y. Li, L. Zhang, Z.T. Yu, K.F. Cen, The effect of concentration on transient pool boiling heat transfer of graphene-based aqueous nanofluids, Int. J. Therm. Sci. 91 (2015) 83-95.

[20] L. Zhang, L. Fan, Z. Yu, K. Cen, An experimental investigation of transient pool boiling of aqueous nanofluids with graphene oxide nanosheets as characterized by the quenching method, Int. J. Heat Mass Transf. 73 (2014) 410-414.

[21] Y. Guo, D. Qin, S. Shen, R. Bennacer, Nanofluid multi-phase convective heat transfer in closed domain: simulation with lattice Boltzmann method, Int. Commun. Heat Mass Transf. 39 (3) (2012)350-354.

[22] M.A. Sheremet, H.F. Oztop, I. Pop, K. Al-Salem, MHD free convection in a wavy open porous tall cavity filled with nanofluids under an effect of corner heater, Int. J. Heat Mass Transf. 103 (2016) 955-964.

[23] M.A. Sheremet, I. Pop, N. Bachok, Effect of thermal dispersion on transient natural convection in a wavy-walled porous cavity filled with a nanofluid: Tiwari

and Das' nanofluid model, Int. J. Heat Mass Transf. 92 (2016) 1053-1060.

[24] X. Liu, Y. Xuan, Full-spectrum volumetric solar thermal conversion via photonic nanofluids, Nanoscale, 9 (39) (2017) 14854-14860.

[25] X.L. Liu, Y.M. Xuan, Defects-assisted solar absorption of plasmonic nanoshell-based nanofluids, Sol. Energy 146 (2017) 503-510.

[26] X.Z. Wang, Y.R. He, G. Cheng, L. Shi, X. Liu, J.Q. Zhu, Direct vapor generation through localized solar heating via carbon-nanotube nanofluid, Energy Convers. Manage. 130 (2016) 176-183.

[27] X. Liu, X. Wang, J. Huang, G. Cheng, Y. He, Volumetric solar steam generation enhanced by reduced graphene oxide nanofluid, Appl. Energ. 220 (2018) 302-312.

[28] M. Sheikholeslami, H.B. Rokni, Nanofluid two phase model analysis in existence of induced magnetic field, Int. J. Heat Mass Transf. 107 (2017) 288-299.

[29] M. Sheikholeslami, Influence of magnetic field on nanofluid free convection in an open porous cavity by means of Lattice Boltzmann method, J. Mol. Liq. 234 (2017) 364-374.

[30] M. Sheikholeslami, D.D. Ganji, Free convection of Fe_3O_4-water nanofluid under the influence of an external magnetic source, J. Mol. Liq. 229 (2017) 530-540.

[31] M. Sheikholeslami, S.A. Shehzad, Z. Li, Water based nanofluid free convection heat transfer in a three dimensional porous cavity with hot sphere obstacle in existence of Lorenz forces, Int. J. Heat Mass Transf. 125 (2018) 375-386.

[32] M. Sheikholeslami, S.A. Shehzad, CVFEM simulation for nanofluid migration in

a porous medium using Darcy model, Int. J. Heat Mass Transf. 122 (2018) 1264-1271.

[33] M. Sheikholeslami, H.B. Rokni, CVFEM for effect of Lorentz forces on nanofluid flow in a porous complex shaped enclosure by means of non-equilibrium model, J. Mol. Liq. 254 (2018) 446-462.

[34] M. Sheikholeslami, S.A. Shehzad, Simulation of water based nanofluid convective flow inside a porous enclosure via non-equilibrium model, Int. J. Heat Mass Transf. 120 (2018): 1200-1212.

[35] M. Sheikholeslami, M. Seyednezhad, Simulation of nanofluid flow and natural convection in a porous media under the influence of electric field using CVFEM, Int. J. Heat Mass Transf. 120 (2018) 772-781.

[36] M. Sheikholeslami, H.B. Rokni, Magnetic nanofluid flow and convective heat transfer in a porous cavity considering Brownian motion effects, Phys. Fluids 30 (1) (2018) 012003.

[37] M. Sheikholeslami, M.M. Bhatti, Forced convection of nanofluid in presence of constant magnetic field considering shape effects of nanoparticles, Int. J. Heat Mass Transf. 111 (2017) 1039-1049.

[38] M. Sheikholeslami, T. Hayat, A. Alsaedi, Numerical simulation of nanofluid forced convection heat transfer improvement in existence of magnetic field using lattice Boltzmann method, Int. J. Heat Mass Transf. 108 (2017) 1870-1883.

[39] M. Sheikholeslami, T. Hayat, A. Alsaedi, S. Abelman, Numerical analysis of EHD nanofluid force convective heat transfer considering electric field dependent

viscosity, Int. J. Heat Mass Transf. 108 (2017) 2558-2565.

[40] M. Sheikholeslami, D.D. Ganji, Impact of electric field on nanofluid forced convection heat transfer with considering variable properties, J. Mol. Liq. 229 (2017) 566-573.

[41] M. Sheikholeslami, M.B. Gerdroodbary, D.D. Ganji, Numerical investigation of forced convective heat transfer of Fe_3O_4-water nanofluid in the presence of external magnetic source, Comput. Methods Appl. Mech. Engrg. 315 (2017) 831-845.

[42] M. Sheikholeslami, S.A. Shehzad, F.M. Abbasi, Z. Li, Nanofluid flow and forced convection heat transfer due to Lorentz forces in a porous lid driven cubic enclosure with hot obstacle, Comput. Methods Appl. Mech. Engrg. 338 (2018) 491-505.

[43] M. Sheikholeslami, CuO-water nanofluid flow due to magnetic field inside a porous media considering Brownian motion, J. Mol. Liq. 249 (2018) 921-929.

[44] M. Sheikholeslami, Numerical investigation for CuO-H_2O nanofluid flow in a porous channel with magnetic field using mesoscopic method, J. Mol. Liq. 249 (2018) 739-746.

[45] S.J. Kline, The description of uncertainties in single sample experiments, Mech. Engg. 75 (1953) 3-9.

[46] B.C. Pak, Y.I. Cho, Hydrodynamic and heat transfer study of dispersed fluids with submicron metallic oxide particles, Exp. Heat Transf. 11 (2) (1998) 151-170.

[47] S.M. Yang, W.Q. Tao, Heat Transfer, 4rd ed., Higher Education Press, Bejing

2012. (in Chinese)

[48] V. Gnielinski, New equations for heat and mass-transfer in turbulent pipe and channel flow, Int. Chem. Eng. 16 (2) (1976) 359-368.

[49] Y. Xuan, W. Roetzel, Conceptions for heat transfer correlation of nanofluids, Int. J. Heat Mass Transf. 43 (19) (2000) 3701-3707.